

See discussions, stats, and author profiles for this publication at: <https://www.researchgate.net/publication/233739254>

Comprehensive chemical kinetic modeling of the oxidation of 2-methylalkanes from C₇ to C₂₀

ARTICLE in COMBUSTION AND FLAME · DECEMBER 2011

Impact Factor: 3.08 · DOI: 10.1016/j.combustflame.2011.05.007

CITATIONS

95

READS

93

14 AUTHORS, INCLUDING:



[C.K. Westbrook](#)

Lawrence Livermore National Laboratory

315 PUBLICATIONS 11,322 CITATIONS

[SEE PROFILE](#)



[Haowei Wang](#)

Rensselaer Polytechnic Institute

13 PUBLICATIONS 396 CITATIONS

[SEE PROFILE](#)



[Matthew A. Oehlschlaeger](#)

Rensselaer Polytechnic Institute

75 PUBLICATIONS 1,607 CITATIONS

[SEE PROFILE](#)



[Ulrich Niemann](#)

University of California, San Diego

20 PUBLICATIONS 555 CITATIONS

[SEE PROFILE](#)



Comprehensive chemical kinetic modeling of the oxidation of 2-methylalkanes from C₇ to C₂₀

S.M. Sarathy ^{a,*}, C.K. Westbrook ^a, M. Mehl ^a, W.J. Pitz ^a, C. Togbe ^b, P. Dagaut ^b, H. Wang ^c, M.A. Oehlschlaeger ^c, U. Niemann ^d, K. Seshadri ^d, P.S. Veloo ^e, C. Ji ^e, F.N. Egolfopoulos ^e, T. Lu ^f

^a Lawrence Livermore National Laboratory, Livermore, CA, USA

^b CNRS-INSIS, 1C Ave de la recherche scientifique - Orléans - France

^c Rensselaer Polytechnic Institute, Troy, NY, USA

^d University of California, San Diego, CA, USA

^e University of Southern California, Los Angeles, CA, USA

^f University of Connecticut, Storrs, CT, USA

ARTICLE INFO

Article history:

Received 25 February 2011

Received in revised form 25 February 2011

Accepted 6 May 2011

Available online 15 June 2011

Keywords:

2-Methylheptane

Iso-alkanes

n-Alkanes

2-Methylalkanes

Chemical kinetic modeling

Mechanism reduction

ABSTRACT

Conventional petroleum jet and diesel fuels, as well as alternative Fischer-Tropsch (FT) fuels and hydro-treated renewable jet (HRJ) fuels, contain high molecular weight lightly branched alkanes (i.e., methylalkanes) and straight chain alkanes (*n*-alkanes). Improving the combustion of these fuels in practical applications requires a fundamental understanding of large hydrocarbon combustion chemistry. This research project presents a detailed and reduced chemical kinetic mechanism for singly methylated iso-alkanes (i.e., 2-methylalkanes) ranging from C₇ to C₂₀. The mechanism also includes an updated version of our previously published C₈–C₁₆ *n*-alkanes model. The complete detailed mechanism contains approximately 7200 species 31400 reactions. The proposed model is validated against new experimental data from a variety of fundamental combustion devices including premixed and non-premixed flames, perfectly stirred reactors and shock tubes. This new model is used to show how the presence of a methyl branch affects important combustion properties such as laminar flame propagation, ignition, and species formation.

Published by Elsevier Inc. on behalf of The Combustion Institute.

1. Introduction

Detailed chemical kinetic combustion models of real fuels (e.g., gasoline, diesel, and jet fuels) are important tools for improving the design, efficiency, and environmental performance of combustion technologies. Fuels derived from conventional petroleum feedstock often are comprised of thousands of different hydrocarbon compounds. This complexity makes it challenging to develop detailed chemical kinetic models of real fuels because modeling each fuel component would be computationally expensive. One way of reducing complexity is to group fuel compounds together into structural classes, and formulate a smaller “surrogate fuel” model that represents the chemical and physical characteristics of the real fuel. In this way the chemical kinetic model becomes easier to build and less computationally expensive to solve in a reacting flow simulation.

Previous studies at the Lawrence Livermore National Laboratory have presented detailed chemical kinetic models for several important structural classes found in real fuels, such as *n*-alkanes [1,2],

iso-alkanes [3–6], alkenes [7,8], aromatics [9], and cyclo-alkanes [10,11]. Surrogate fuel models have also been developed for gasoline fuel [9,12] and for primary reference fuels of gasoline and diesel [13] by merging the models of relevant structural classes. A recent review paper by Pitz and Mueller [14] describes the development of diesel surrogate fuel models. The composition of typical diesel fuels is presented as a mixture of high molecular weight (i.e., C₁₀–C₂₀) *n*-alkanes, lightly branched iso-alkanes with one or two methyl groups, cycloalkanes with multiple alkyl side chains, and aromatics with multiple side chains. The recent progress in combustion modeling of these structural classes is discussed in detail; however, the authors conclude that major research gaps remain in modeling high molecular weight (i.e., greater than C₁₀) aromatics, alkyl aromatics, cyclo-alkanes, and lightly branched iso-alkanes.

The focus of the present research study is on high molecular weight 2-methylalkanes from C₈ to C₂₀. n-Alkyl radicals are important intermediates in the combustion of 2-methylalkanes, so this study also presents an updated version of our previously published C₈–C₁₆ *n*-alkanes model [2], wherein the core chemistry mechanism is updated, new reaction classes are added, and important rate rules are updated (i.e., refer to Section 2 for details). 2-methylalkane and *n*-alkane structures are important components of

* Corresponding author.

E-mail address: sarathy1@llnl.gov (S.M. Sarathy).

conventional diesel fuels derived from petroleum [14,15], synthetic Fischer-Tropsch diesel and jet fuels derived from coal, natural gas, and/or biomass [16,17], and renewable diesel and jet fuels derived from thermochemical treatment of bio-derived fats and oils (e.g., hydrotreated renewable jet (HRJ) fuels) [18,19]. Significant effort is placed on understanding the effect of carbon chain length and methyl substitution along the chain on important combustion properties.

1.1. Previous combustion studies on 2-methylalkanes

Limited research has been performed on the fundamental combustion properties of 2-methylalkanes. *iso*-Butane (2-methylpropane, iC₄H₁₀) has been studied in engines by Wilk et al. [20] and in shock tubes by Ogura et al. [21], Oehlschlaeger et al. [22], and Healy et al. [23]. Burcat et al. [24] studied the high temperature shock tube autoignition of 2-methylpentane (C₆H₁₄-2). Several experimental and kinetic modeling studies have been performed on 2-methylhexane (C₇H₁₆-2) by Westbrook et al. [5,6], Griffiths et al. [25], and Silke et al. [26]. 2-Methylheptane (C₈H₁₈-2) has been studied by Kahandwala et al. [27] in high temperature shock tubes. Sarathy et al. [28] recently presented a high temperature chemical kinetic model for 2-methylheptane and validated it against counterflow diffusion flame species profiles. In summary, the aforementioned studies conclude the 2-methylalkanes are less reactive under autoignition conditions than *n*-alkanes of the same chain length. At lower temperatures and in the negative-temperature-coefficient (NTC) region, the decreased reactivity is attributed to depressed RO₂ isomerization reactions in the branched alkane; and at high temperatures, the branch alkanes are less reactive since they lead to the unreactive resonantly stabilized allyl (C₃H₅) radical, via propene (C₃H₆) [21], and methyl allyl (iC₄H₇, *iso*-butenyl) radical, via *iso*-butene. The flame studies reveal that 2-methylalkanes produce more branched alkenes (i.e., 2-methylalkenes) and propene due to the presence of a tertiary C-H bond [28].

1.2. Ignition quality of 2-methylalkanes

A fuel's autoignition properties are typically quantified using the familiar octane and cetane scales. In both scales, an *n*-alkane is used as a reference compound for the most easily ignited fuel (i.e., *n*-heptane and *n*-hexadecane), while a highly branched alkane is used as reference compound for the least easily ignited fuel (i.e., *iso*-octane and 2,2,4,4,6,8,8-heptylmethylnonane). The high ignition quality of *n*-alkanes is attributed to their low temperature reactivity, which leads to degenerate chain branching and early heat release. On the other hand, the poor ignition quality of highly branched alkanes is due to the inability of these compounds to lead to degenerate chain branching under low temperature oxidation conditions.

One goal of the present study is to elucidate the effects of methyl branching on the autoignition properties of 2-methylalkanes by comparing their reactivity with *n*-alkanes of the same chain length. A simple and practical method of comparing the ignition quality of two fuels is to compare their derived cetane numbers (DCN) using the ASTM 6890 method [29] in an ignition quality tester (IQT) [30,31].

Table 1 presents unpublished NREL IQT test data for two *n*-alkanes (i.e., *n*-heptane and *n*-octane) and their 2-methylalkane counterparts (i.e., 2-methylhexane and 2-methylheptane). The results indicate that 2-methylalkanes are slower to ignite than *n*-alkanes of the same chain length. These results are consistent with the general understanding that alkane branching decreases the ignition quality of a fuel. The present study will attempt to further clarify the differences in autoignition quality of *n*-octane versus 2-

Table 1
Derived cetane number (DCN) values for *n*-alkanes and 2-methylalkanes.

Compound	Ignition delay (ms), NREL ^a	DCN, NREL ^a
<i>n</i> -Heptane (<i>n</i> C ₇ H ₁₆)	3.784	53.8
2-Methylhexane (C ₇ H ₁₆ -2)	4.775	43.5
<i>n</i> -Octane (<i>n</i> C ₈ H ₁₈)	3.513	57.6
2-Methylheptane (C ₈ H ₁₈ -2)	3.881	52.6

^a Unpublished results from the National Energy Renewable Laboratory 2007–2010; all DCNs from D6890-06 equation; DCN = 4.460 + 186.6/ID.

methylheptane using fundamental shock tube autoignition data and detailed chemical kinetic modeling simulations.

2. Chemical kinetic mechanism formulation

The proposed detailed chemical kinetic mechanism includes both low-temperature and high-temperature kinetic schemes for 2-methylalkanes from C₇ to C₂₀. We include the important reaction pathways based on the early work of Curran et al. on *n*-heptane and *iso*-octane [1,3]. In addition, we include an updated version of our C₈–C₁₆ *n*-alkane sub-mechanism initially developed by Westbrook et al. [2]. The data files for the complete model include a detailed chemical kinetic reaction mechanism, a dataset of thermochemical properties, and a dataset of transport properties. The entire model consists of approximately 7200 species and 31,400 reactions. These input files are available as supplemental material to this publication and from our website at: https://www-pls.llnl.gov/?url=science_and_technology-chemistry-combustion.

The “core mechanism” used here is our latest detailed mechanism for *n*-heptane, which was presented and discussed as part of the gasoline surrogates model by Mehl et al. [9,12]. This core mechanism is comprised of an updated C₀–C₅ sub-mechanism [32,33], the C₆–C₇ alkane sub-mechanism from Mehl et al. [9,12], and the C₅–C₇ alkenes sub-mechanism from Mehl et al. [7,8]. We found the following two errors in the C₀–C₅ sub-mechanism that were corrected to obtain converged counter-flow flame simulations:

- The reaction ch2(s) ⇌ ch2 was changed to ch2(s) + m ⇌ ch2 + m and is consistent with the current bi-molecular rate constant expression.
- The specified reverse rate for the reaction o + c2h2 ⇌ c2h + oh was above the collisional limit at 300 K, so the rate was changed to have an A factor of 9 × 10¹³ with no temperature dependence.

We initiated the present work by building a high-temperature mechanism for the C₈ 2-methylalkane (i.e., 2-methylheptane), which was previously discussed by Sarathy et al. [28]. The 2-methylheptane mechanism was built in a modular fashion, starting with the high temperature reactions (i.e., classes 1–10) for 2-methylhexane described by Westbrook et al. [5,6], and subsequently adding the analogous pathways for 2-methylheptane. This study follows a similar methodology to develop the high-temperature reaction pathways for 2-methylalkanes up to C₂₀. As a result, the mechanism requires high-temperature reaction pathways for *n*-alkyl radicals up to C₁₉ as well. The C₈–C₁₆ *n*-alkyl species, are already present in the C₈–C₁₆ *n*-alkane sub-mechanism from Westbrook et al. [2], so we only add the relevant high-temperature reaction classes (i.e., classes 3–9) for C₁₇–C₁₉ *n*-alkyl species.

The low-temperature reaction pathways for 2-methylalkanes (i.e., low temperature classes 11–30) are written starting with those for 2-methylhexane from Westbrook et al. [2]. The analogous pathways are then written for all 2-methylalkanes from C₈ to C₂₀.

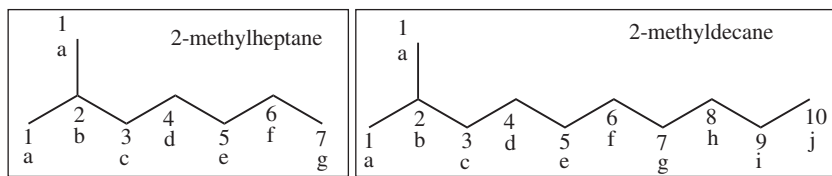


Fig. 1. Structure of 2-methylheptane ($C_8H_{18}-2$) and 2-methyldecane ($C_{11}H_{24}-2$).

Several modifications are made to the reaction pathways and reaction rate rules presented in our previous hydrocarbon mechanisms [1–3] to make the proposed mechanism consistent with our recent gasoline surrogates mechanism [9,12] and to better agree with the experimental data presented herein.

2.1. Naming of species

To illustrate the naming of the species for the 2-methylalkanes mechanism, 2-methylheptane is denoted as $C_8H_{18}-2$ in the mechanism, for example (see Fig. 1 for its molecular structure). The carbon chain is labeled numerically (i.e., 1, 2, 3, etc.) such that the location number of the methyl branch is minimized. For 2-methylheptene species, the location of a double bond is identified by a hyphen followed by the number of the first carbon in the double bond (e.g., 2-methyl-3-heptene is $C_8H_{16}-3-2$). Additional notations are provided to denote radical sites in the molecule. The carbon sites are labeled alphabetically (i.e., a, b, c, etc.) such that the location of the first methyl branch is minimized (Fig. 1). In this way, the 2-methyl-3-heptyl radical is denoted as $C_8H_{17}-2c$, while the 2-methyl-1-heptyl radical is written as $C_8H_{17}-2a$. For larger 2-methylalkanes, the same naming convention is used with added letters and numbers to account for the additional carbons on the chain. For example, the structure and naming convention of 2-methyldecane is given in Fig. 1.

2.2. Classes of reactions

The major classes of elementary reactions considered for the oxidation of C_8 – C_{16} *n*-alkanes and C_7 – C_{20} 2-methylalkanes include the following:

High Temperature Reaction Classes:

1. Unimolecular fuel decomposition.
2. H-atom abstraction from the fuel.
3. Alkyl radical decomposition.
4. Alkyl radical isomerization.
5. H-atom abstraction reactions from alkenes.
6. Addition of radical species O and OH to alkenes.
7. Reactions of alkenyl radicals with HO_2 , CH_3O_2 , and $C_2H_5O_2$.
8. Alkenyl radical decomposition.
9. Alkene decomposition.
10. Retroene decomposition reactions.

Low Temperature Reaction Classes:

11. Addition of O_2 to alkyl radicals ($R + O_2 = ROO$).
12. $R + ROO = RO + RO$.
13. $R + HO_2 = RO + OH$.
14. $R + RO_2ROO = RO + RO$.
15. Alkyl peroxy radical isomerization ($ROO = QOOH$).
16. Concerted eliminations ($ROO = \text{alkene} + HO_2$).
17. $ROO + HO_2 = ROOH + O_2$.
18. $ROO + H_2O_2 = ROOH + HO_2$.
19. $ROO + CH_3O_2 = RO + CH_3O + O_2$.
20. $ROO + ROO = RO + RO + O_2$.

21. $ROOH = RO + OH$.
22. RO decomposition.
23. $QOOH = \text{cyclic ether} + OH$ (cyclic ether formation).
24. $QOOH = \text{alkene} + HO_2$ (radical site beta to OOH group).
25. $QOOH = \text{alkene} + \text{carbonyl} + OH$ (radical site gamma to OOH group).
26. Addition of O_2 to $QOOH$ ($QOOH + O_2 = OOQOOH$).
27. Isomerization of $OOQOOH$ and formation of carbonylhydroperoxide and OH.
28. Decomposition of carbonylhydroperoxide to form oxygenated radical species and OH.
29. Cyclic ether reactions with OH and HO_2 .
30. Decomposition of large carbonyl species and carbonyl radicals.

2.3. Description of chemical kinetic mechanism

Curran et al. [1,3] have discussed many of the aforementioned reaction classes. For the sake of brevity, this section presents a list summarizing the most notable updates to reaction classes and reaction rate constants in the proposed model. For readers seeking a comprehensive description, we direct them to the [Supplementary material](#), where each reaction class, the chosen rate constants, and their sources are described in detail. The most significant model developments are as follows:

- Alkyl radical decomposition (i.e., class 3) and isomerization (i.e., class 4) rates are based on recent kinetic studies at the National Institute of Standards and Technology (NIST) [34–37]. The introduction of these rate constants improved species profile prediction in a previous study on opposed-flow diffusion flames of 2-methylheptane and *n*-octane [28].
- The reaction rate constants for alkyl peroxy radical isomerization (i.e., low temperature class 15) are from our latest *n*-heptane model by Mehl et al. [9]. The rates are originally from Curran et al. [1], but the activation energies are reduced by 400 cal/mol to follow the recommendations of Zhu et al. [38], and to obtain better agreement in previous work on ignition of *n*-heptane [9]. These new rates increase low temperature reactivity below 700 K and predict shorter ignition delays compared to our previous *n*-alkane mechanism [2].
- We include a new reaction path, not included in our previous *n*-alkanes work [2], of the molecular elimination of HO_2 from ROO (i.e., class 16). This concerted (i.e., direct) elimination of HO_2 from the alkyl peroxy radical (i.e., ROO) occurs via a 5-membered transition state and was first discovered by Quelch et al. [39] and also well studied by [40,41]. This reaction class was included in our latest *n*-heptane/iso-octane model by Mehl et al. [9] and our cyclohexane model by Silke et al. [42], but we have updated the rate constants in the present study.
- The addition of the concerted elimination reactions depresses reactivity in the NTC region, so the rate of chain branching reactions was increased to compensate for the addition of the former. The reaction rate constants for carbonylhydroperoxide decomposition (i.e., class 28) are from our latest *n*-heptane

model by Mehl et al. [9]. The activation energy for these reactions was decreased from the work of Curran et al. [1] to better predict low temperature ignition delay times for *n*-heptane [9].

In summary, many of the updates made to our previous *n*-alkane model were done to obtain consistency with our latest *n*-heptane model. The new reaction classes and reaction rates were updated based on the latest findings from various combustion researchers. We tested the *n*-alkane reactivity of the updated model against the previous model and found that ignition delay times were quantitatively similar except at temperatures below 700 K. Although not explicitly presented in this study, the proposed model has the same predictive quality as our previous *n*-alkane model [2].

2.4. Thermochemical data

The thermodynamic parameters for the species are very important because they are used to determine reverse rate constants. The THERM [43] software is used to compute the thermochemical properties of species not present in the *n*-alkane model [2]. The THERM group values are from Benson [44] and Bozzelli [45,46].

2.5. Transport properties

Kinetic processes and transport processes are rate controlling in diffusion flames and droplet vaporization/combustion, so transport properties are needed for all the species in the model. This study obtains the molecular transport parameters for species using a variety of methods. The transport properties for species up to C₈ are already available in a previously published 2-methylheptane model [28]. The transport properties of larger alkanes, alkene, alkyl, and alkenyl species are determined as follows. For stable species, this study uses the correlations developed by Tee, Gotoh, and Stewart [47], as first described by Wang and Frenklach for aromatics [48], and later by Holley and coworkers for hydrocarbons [49], to calculate the LJ collision diameter and potential well depth using the critical pressure (P_c), critical temperature (T_c), and acentric factor (ω). The estimation of the acentric factor (ω) is based on Lee-Kesler vapor-pressure relations [50], which requires the critical pressure (P_c), critical temperature (T_c), and boiling point (T_b) of the species. P_c , T_c , and T_b for the majority stable species are based on the recommendations of Owczarek and Blazej [51,52], which provide all the data values for *n*-alkanes up to C₂₀, 2-methylalkanes up to C₁₁, and partial data for 1-alkenes up to C₂₀. No data was available for 2-methylalkanes from C₁₂ to C₂₀; however, a strong correlation exists between carbon chain length and P_c , T_c , and T_b for 2-methylalkanes up to C₁₁, so we extrapolate these values for larger 2-methylalkanes using a power law function, as shown in Supplementary Fig. S1. A similar method is followed to determine missing data for 1-alkenes.

Following previous work [53], the polarizability in cubic Angstroms of stable species is calculated using an empirical correlation [54], which depends on the number of C, H, and O atoms in the molecule. The values calculated using this method are comparable to experimentally measured polarizability for species where such data is available [55]. The dipole moment for all new species is set to zero because they are non-polar hydrocarbons [56]. The index factor which describes the geometry of the molecule is determined from the molecular structure (i.e., 0 for atoms, 1 for linear molecules, and 2 for nonlinear molecules). We attempt to calculate different transport properties for alkanes and alkenes of the same chain length according to their differences in corresponding states (e.g., P_c , T_c , and T_b); however, sufficient data was unavailable for large 2-methylalkenes, so we use the transport parameters of the

corresponding 2-methylalkane. For alkyl and alkenyl radical species, the transport properties of their stable counterpart are used.

We also include a rough estimation of transport properties for species in the low temperature mechanism (i.e., RO, RO₂, ROOH, QOOH, cyclic ethers, etc.) by assuming the transport properties are the same as the parent fuel molecule from which they are derived. We acknowledge that this is a poor assumption, but practically we do not expect it to significantly affect simulations since the concentrations of these low temperature species are small and the reactivity of the system is typically driven by the fuel's transport properties. Nevertheless, we caution researchers interested in using our chemical kinetic model to test the sensitivity of their results on our proposed transport parameters.

3. Validation studies

The proposed model for large *n*-alkanes and 2-methylalkanes has been validated against a wide range of experimental data. Westbrook et al. [2] previously validated the C₈–C₁₆ *n*-alkane mechanism; the present improvements to the reaction classes and rate rules do not significantly alter the validations presented previously. In this study, we include additional new validations for *n*-alkanes, but the focus is on validation data for 2-methylalkanes. The experimental focus is on 2-methylheptane since this molecule is easy to work with experimentally (i.e., less expensive and lower boiling point than larger 2-methylalkanes). Validating the mechanism against 2-methylheptane is considered adequate because the same reaction rate rules are applied for larger 2-methylalkanes. The following is a list specific validation studies performed:

1. Low and intermediate temperature rapid compression machine (RCM) ignition data for 2-methylhexane by Silke et al. [26].
2. Jet stirred reactor species profiles data for 2-methylheptane performed in this study at CNRS, Orleans.
3. Low and high temperature shock tube ignition data for 2-methylheptane and *n*-octane performed in this study at the Rensselaer Polytechnic University.
4. Premixed laminar flame velocity data for *n*-octane by Ji et al. [57] and Kelley et al. [58] and for 2-methylheptane performed in this study at the University of Southern California with simulations performed using a high-temperature C₈ version of the detailed mechanism, wherein species greater than C₈ and reaction classes 11–30 were removed.
5. Counterflow diffusion flame extinction and ignition data for 2-methylheptane performed in this study by at the University of California San Diego with simulations performed using a skeletal mechanism prepared at the University of Connecticut.

One challenge for this work was that no experimental data were available for any 2-methylalkanes with greater than 8 C atoms. A similar challenge was encountered in our recent kinetic modeling study of *n*-alkane combustion [2] for fuels up to *n*-hexadecane, where little validation data were available for fuels with more than 10 C atoms. This difficulty arises because vapor pressures of these large hydrocarbon fuels are very low, making well-characterized gas-phase experiments very difficult. Interestingly, experiments subsequent to publication of that paper [59,60] showed excellent agreement with the modeling predictions, indicating that the systematic extensions of the rule-based kinetic mechanisms from smaller molecules, for which validation data was available, to larger fuels with the same structure, where data were not yet available, could be made with some confidence. In the present study, several experimental groups were able to contribute new experimental data for mechanism validation for 2-methylheptane, as

discussed below. For the even larger fuel molecules, as done in our previous *n*-alkane kinetic study, the mechanisms for the 2-methylalkanes with more than 8 C atoms are used to carry out kinetic modeling exercises to illustrate the trends predicted by the kinetic models. As described below, predicted kinetic trends for these larger 2-methylalkanes are consistent with known trends in the experimentally measured cetane numbers for these fuels. Additional experimental studies are needed to provide further tests of the present 2-methylalkane mechanisms, particularly for the larger fuels, but the present models provide a realistic means of including this class of fuels in surrogate and other models of practical transportation fuels including gasoline, jet fuels and diesel fuels.

3.1. Rapid compression machine (RCM) experiments and simulations for 2-methylhexane

This section uses a detailed chemical kinetic mechanism for 2-methylhexane to simulate ignition in a RCM. Westbrook et al. [5] and Silke et al. [26,61] present RCM ignition data of 2-methylhexane in two separate experimental facilities. The present study uses the data obtained by Silke et al. [26,61] to validate the proposed mechanism.

3.1.1. RCM results

The Galway RCM experiments by Silke et al. [26,61] were obtained at an equivalence ratio of $\phi = 1$ (21% O₂, 79% diluent) and an end of compression pressures (P_c) in the range 13.5–15 atm. The initial pressure (P_i), initial temperature (T_i), and diluent gas composition (i.e., concentrations of Ar and N₂) were initially set to achieve the desired P_c and end of compression temperature (T_c). The experiments were conducted at a compression time (t_c) of 16.6 ms, and the compression ratio (CR) was in the range 9.5–10.2 depending on the diluent gas composition. The actual P_c was measured for each experimental run, and then T_c was calculated based on ideal gas theory. The ignition delay time (τ_{id}) was defined as the time of maximum pressure rate rise (dP/dt) after the end of compression. Further details of the experimental setup and raw experimental data are available in Silke's thesis [61].

The present RCM kinetic modeling simulations were performed in CHEMKIN PRO [62] using the homogenous batch reactor code to

model the entire compression stroke using the P_i , T_i , CR, and t_c . The experimental CR varied slightly with each run, so we assumed a CR of 10 for all simulations. Heat losses in the RCM are usually modeled by using the technique of "heat loss mapping" as described by Dooley et al. [63]; however, a non-reactive pressure trace was not available for conditions similar to the present study (e.g., CR 10), so we were unable to model heat losses after the end of compression. The onset of ignition was determined as the point of maximum temperature rise (max dT/dt), which corresponds closely to the point of maximum pressure rate rise (max dP/dt). The simulated τ_{id} is plotted against the predicted T_c for each simulation run.

The Galway RCM experimental and simulation results are presented in Fig. 2. The ignition delay time is plotted against the temperature at the end of compression. The experimentally measured ignition delay times are presented as solid triangles. The simulation data is plotted as a line with open triangles. Overall the model exhibits good agreement in trend with the experimental data. At all temperatures the simulation predicts ignition delay times within two times of the experimental values. The agreement between simulated and experimental data improves as the temperature increases, and above 750 K there is a very good agreement. Minor negative temperature coefficient behavior is observed in both the experiments and simulations from 750 to 900 K. It should be noted that incorporating heat loss considerations into the simulations may increase predicted ignition delay times below 700 K by as much as a factor of 1.5; at higher temperatures there would be little change in the predicted ignition delay times.

3.2. Jet stirred reactor (JSR) experiments and simulations for 2-methylheptane

The jet stirred reactor is a fundamental experimental tool for understanding the low temperature and high temperature reactivity of 2-methylheptane, as well as the major and minor species formed at various temperatures and equivalence ratios. The experiments presented herein were conducted at high pressure (i.e., 10 atm) to better study the low temperature reactivity of 2-methylheptane under conditions similar to those found in internal combustion engines. This new experimental dataset is used to validate the proposed model and its reaction rate rules used for modeling 2-methylalkanes up to C₂₀.

3.2.1. JSR experimental setup

We used the JSR experimental setup utilized in previous studies [64,65]. It consisted of a small spherical fused-silica reactor (4 cm outside diameter) equipped with four nozzles of 1 mm I.D. each. High-purity reactants were used in the present experiments: oxygen (99.995% pure) and 2-methylheptane (>99%). The reactants were diluted with nitrogen (<100 ppm H₂O) and quickly mixed before admission into the injectors. To minimize temperature gradients within the JSR, the reactants were preheated. A Shimadzu LC10 AD VP pump operating with an on-line degasser (Shimadzu DGU-20 A3) was used to distribute the fuel to an in-house atomizer-vaporizer assembly thermally regulated at 473 K. A high degree of dilution (0.15–0.2% mol. of fuel) was used to reduce heat release and temperature gradients inside the JSR. Temperatures were measured by a 0.1 mm Pt-Pt/Rh-10% thermocouple located inside a thin-wall silica tube to avoid catalytic effects. A movable low-pressure fused silica sonic probe was used to sample the reacting mixtures inside the JSR. The samples were transferred to analyzers via a Teflon heated line (473 K). They were analyzed online by FTIR (cell: 10 m path length and 200 mbar; spectral resolution of 0.5 cm⁻¹) and off-line, after collection and storage in 1 L Pyrex bulbs. Gas chromatographs (GC) equipped with capillary columns (DB-624 for oxygenates, CP-Al₂O₃-KCl for hydrocarbons, and Carboplot-P7 for hydrogen and oxygen), a TCD (thermal

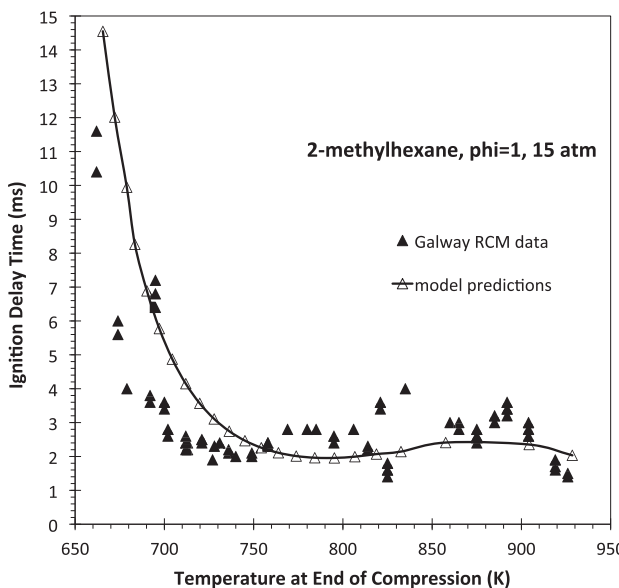


Fig. 2. Experimental (Silke et al. [26]) and simulated ignition delay times for 2-methylhexane. $P = 15$ atm, $\phi = 1.0$.

conductivity detector), and an FID (flame ionization detector) were used for off-line analyses. Products identification was performed by means of a GC-MS (Varian V1200) operated with electron ionization (70 eV). Fragmentation patterns were compared to data obtained in previous work [66].

The experiments were performed at steady state, at a constant pressure of 10 atm and a constant mean residence time, τ , of 0.7 s. The reactants flowed constantly into the JSR and the temperature of the gases inside the reactor was increased stepwise. A good repeatability of the measurements and a reasonably good carbon balance were obtained in this series of experiments (e.g., $100 \pm 10\%$ at low and high temperatures, and $100 \pm 20\%$ in the NTC region since minor oxygenates were not measured). Uncertainties for all species concentration measurements were 10%, except for cyclic ether concentration which had a 15% error. Temperature gradients of $<7\text{ K/cm}$ along the vertical axis of the reactor were recorded, and the reported temperature is the average along the vertical axis with an error of $\pm 4\text{ K}$.

3.2.2. JSR results

The CHEMKIN PRO [62] transient perfectly stirred reactor code was used to validate the proposed kinetic model against jet stirred reactor data for 2-methylheptane at 10 atm, three equivalence ratios ($\phi = 0.5$, $\phi = 1.0$, and $\phi = 2.0$), and a range of temperatures between 500 and 1200 K. The JSR allows us to study the oxidation of 2-methylheptane in a flameless premixed environment. Sonic probe sampling and GC and FTIR analyses measured the concentration of species at each equivalence ratio and temperature condition. The important measured species are 2-methylheptane ($C_8H_{16}-2$), hydrogen (H_2), oxygen (O_2), water (H_2O), carbon monoxide (CO), carbon dioxide (CO_2), methane (CH_4), ethane (C_2H_6), acetylene (C_2H_2), ethylene (C_2H_4), ethane (C_2H_6), propene (C_3H_6), ethanal (CH_3CHO), formaldehyde (CH_2O), propanal (C_2H_5CHO), acetone (CH_3COCH_3), 2-propenal (C_2H_3CHO), butanal (C_3H_7CHO), 1-butene ($1-C_4H_8$), iso-butene (iC_4H_8), 1,3-butadiene ($1,3-C_4H_6$), 1-pentene ($C_5H_{10}-1$), 2-methyl-3-butene ($C_5H_{10}-3-2$ aka 3-methyl-1-butene), 2-methyl-1-heptene ($C_8H_{16}-1-2$), 2-methyl-2-heptene ($C_8H_{16}-2-2$), 2-methyl-5-isopropyl-tetrahydrofuran ($C_8H_{16}O_3-6-2$), 5-ethyl-2,2-dimethyl-tetrahydrofuran ($C_8H_{16}O_2-5-2$), and 3-methyl-5-propyl-tetrahydrofuran ($C_8H_{16}O_1-4-2$). Measured species with maximum concentrations below 10 ppm were considered unimportant, and these include 3-methylbutanal, pentanal, propane, *trans*-2-butene, *cis*-2-butene, cyclo-pentane, *trans*-2-pentene, *cis*-2-pentene, 2-methyl-4-pentene (aka 4-methyl-1-pentene), 2-methyl-2-hexene, 2-methyl-3-heptene, 2,2-dimethyl-5-propyl-oxetane, 2-methyl-5-isopropyl-tetrahydrofuran, 3-methyl-5-propyl-tetrahydrofuran, 2-isobutyl-tetrahydrofuran. Experimental data for all the aforementioned species are reported available in the Supplementary material.

Figure 3 presents the experimental measurements with error bars (i.e., based on uncertainties mentioned above) and modeling results of 2-methylheptane obtained at $\phi = 1.0$. The experimental results (symbols) show that with increasing temperature, the 2-methylheptane concentration drops significantly between 500 K and 650 K. This corresponds to the cool flame reactivity regime, wherein the overall low temperature peroxy sequence is active leading to chain branching. In this region, the first maximum of several oxygenated compounds (e.g., CO, H_2O , CH_2O , acetone, propanal, 2-propenal, and ethanal) is created from the decomposition of ketohydroperoxide species. From 650 K to 750 K, there is an increase in the 2-methylheptane concentrations exhibiting the negative temperature coefficient (NTC) behavior of the system wherein the concerted elimination reactions and cyclic ether formation are dominant. The cyclic ether species (i.e., furans) reach their peak concentration in this temperature region. Above 750 K, the fuel concentration decreases continuously as low temperature

reaction pathways become less important, and high temperature kinetics control the systems reactivity. Many alkene species reach their maximum concentration around 850 K and are then destroyed at higher temperature. 850 K also corresponds to a second maximum in the concentration of small oxygenates.

The model predictions (lines) for $\phi = 1.0$ are also shown in Fig. 3. The model's ability to reproduce the experimental data is discussed qualitatively and quantitatively. The model's prediction is considered good if the shape of the model profile closely matches the experimental profile, and if the predicted maximum mole fraction is within a factor 2 of the measured maximum mole fraction. The concentration of the reactants of 2-methylheptane and O_2 is well predicted at all temperatures, and so is the concentration of the major product species CO , CO_2 , and H_2O . The model well predicts the minor species CH_4 , H_2 , C_2H_2 , and C_2-C_8 unsaturated hydrocarbons (i.e., alkenes and dienes). The concentration of oxygenated product species CH_2O and ethanal is well predicted, but 2-propenal is over predicted and butanal is under predicted. The first maximum concentration (i.e., peak) of acetone is well predicted by the model, but the model under predicts the second peak. This discrepancy is related to the formation of acetone from iso-butene, which is a reaction sequence that needs further analysis.

The cyclic ether species measured in the JSR are all furans (i.e., 5-membered rings), and the model also predicts that these are the predominant cyclic ether species. This is consistent with the recent findings of Herbinet et al. in their experimental study cyclic ethers formed in the low-temperature oxidation of a series of *n*-alkanes [67]. In the present study, the model well predicts the profiles of the furans; however, the concentration of 2-methyl-5-isopropyl-tetrahydrofuran is over predicted.

Figures 4 and 5 present the experimental and modeling results obtained at $\phi = 0.5$ and $\phi = 2.0$ in the JSR, respectively. For clarity, error bars are not presented on these figures. The experimental data and model predictions show a similar trend as observed at $\phi = 1.0$. Overall the model predictions are in excellent agreement with the JSR data, especially considering the two studies were conducted separately and not optimized for good agreement.

3.3. Shock tube autoignition experiments and simulations of *n*-octane and 2-methylheptane

Studying the autoignition of 2-methylalkanes and *n*-alkanes under similar conditions can elucidate the effects of fuel molecular structure on low temperature reactivity. It has been shown that 2-methylalkanes have lower cetane numbers than *n*-alkanes of the same chain length. Therefore, the low temperature and negative temperature coefficient (NTC) reactivity of 2-methylalkanes is expected to be lower than *n*-alkanes. Shock tube autoignition studies enable us to study the low temperature and NTC reactivity under idealized conditions. This section presents new experimental data for *n*-octane and 2-methylheptane at 20 atm and a range of equivalence ratios, and uses the data to validate the proposed chemical kinetic model.

3.3.1. Shock tube experimental setup

Ignition delay times were measured for 2-methylheptane and *n*-octane in reflected shock experiments performed in a heated high-pressure shock tube at Rensselaer Polytechnic Institute. The shock tube has been previously described in detail [59]. The heated shock tube temperature ($\sim 100\text{ }^\circ\text{C}$) was chosen to be sufficiently high to avoid fuel condensation and provide ease of gaseous fuel/air mixture preparation and sufficiently low to avoid fuel decomposition during mixture preparation. Measurements of the axial uniformity of the driven section inner wall temperature revealed that the driven section temperature variation was at $\pm 2\text{ }^\circ\text{C}$.

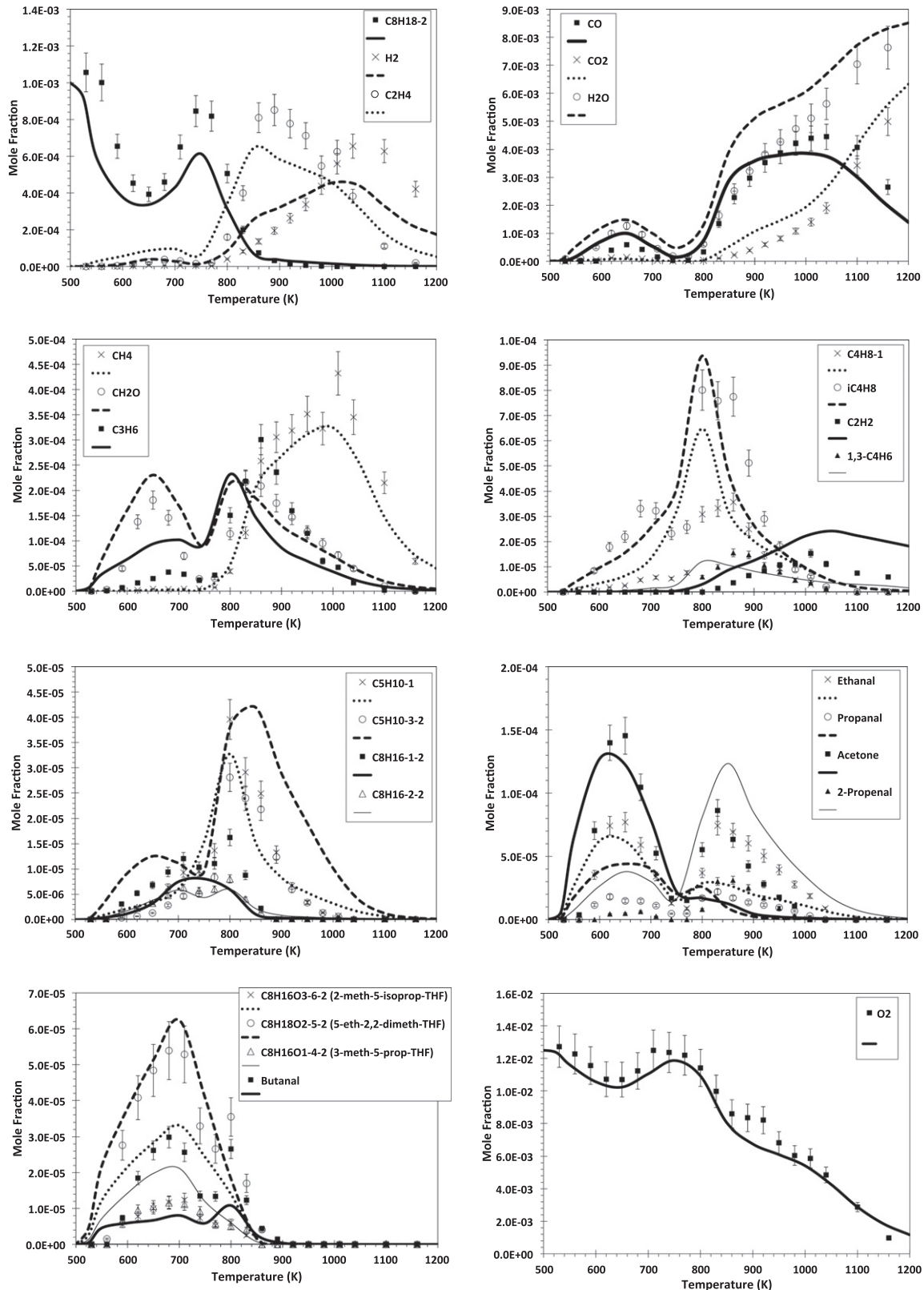


Fig. 3. 2-Methylheptane oxidation in a JSR at 10 atm, $\tau = 0.7$ s and $\phi = 1.0$. The initial fuel ($C_8H_{18}-2$) mole fraction was 0.1%. Experimental data (symbols) with error bars are compared to calculations (lines).

2-Methylheptane/air and *n*-octane/air mixtures were prepared by direct injection of the liquid fuels into a heated mixing vessel followed by complete fuel evaporation, monitored via pressure, and the addition of O_2 and N_2 from compressed gas cylinders, at

a molar ratio of 1:3.76. Fuel, O_2 , and N_2 mixture fractions were specified via partial pressures. Liquid 2-methylheptane was procured from Eastern Sources at 99+% purity, liquid *n*-octane from Sigma Aldrich at 99+% purity, and O_2 and N_2 from Noble Gas

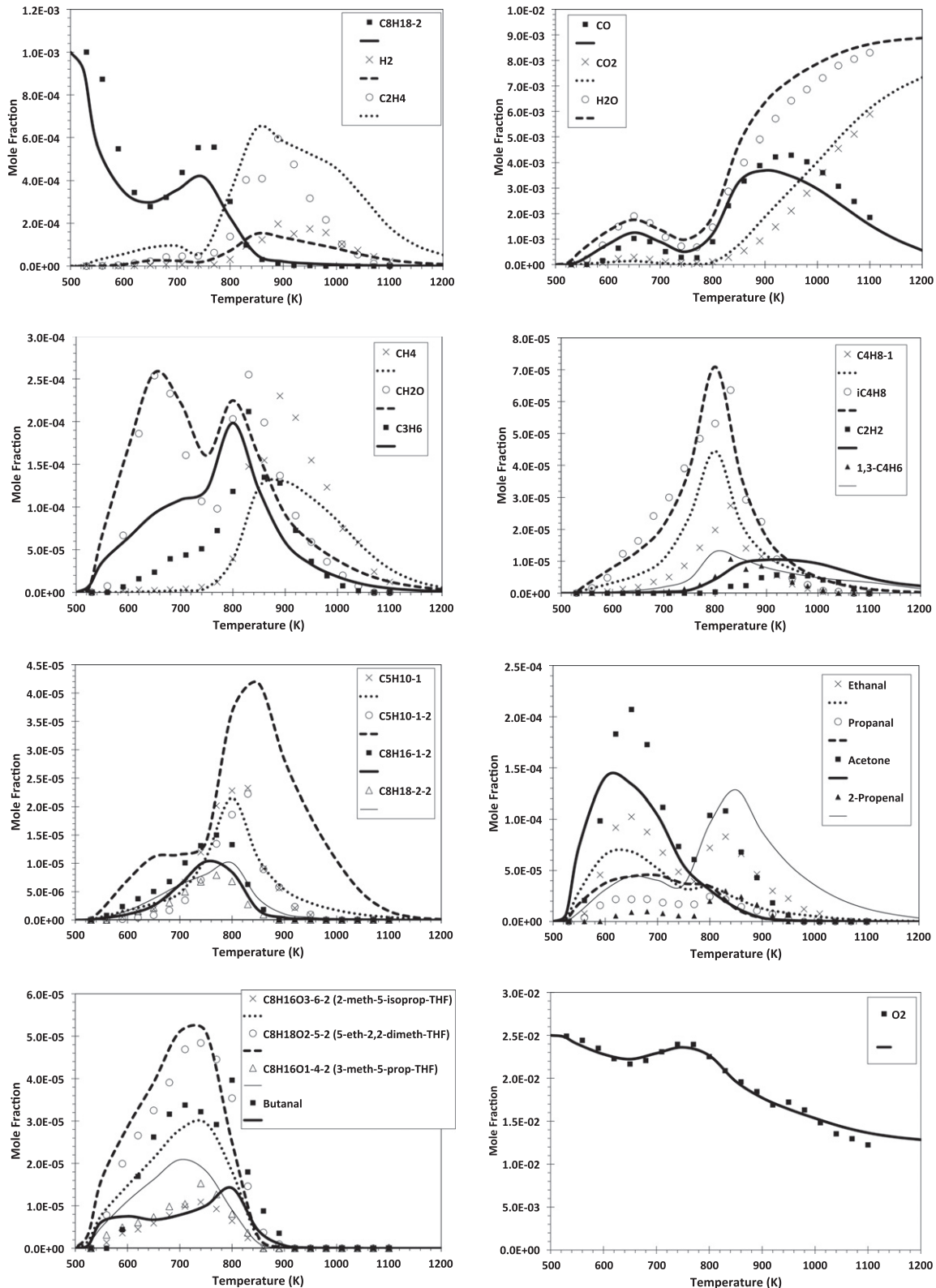


Fig. 4. 2-Methylheptane oxidation in a JSR at 10 atm, $\tau = 0.7$ s and $\phi = 0.5$. The initial fuel ($C_8H_{18}-2$) mole fraction was 0.1%. Experimental data (symbols) are compared to calculations (lines).

Solutions both at 99.995% purity. Fuel/air mixtures were mechanically mixed inside the heated mixing vessel with a magnetically powered vane assembly for 20 min to 4 h prior to shock tube autoignition experiments.

Reflected shock ignition delay time measurements were made for 2-methylheptane/air and *n*-octane/air mixtures at equivalence ratios of 0.5, 1.0, and 1.5 at pressures near 20 atm and for temperatures from 631 to 1327 K. To provide sufficient test times

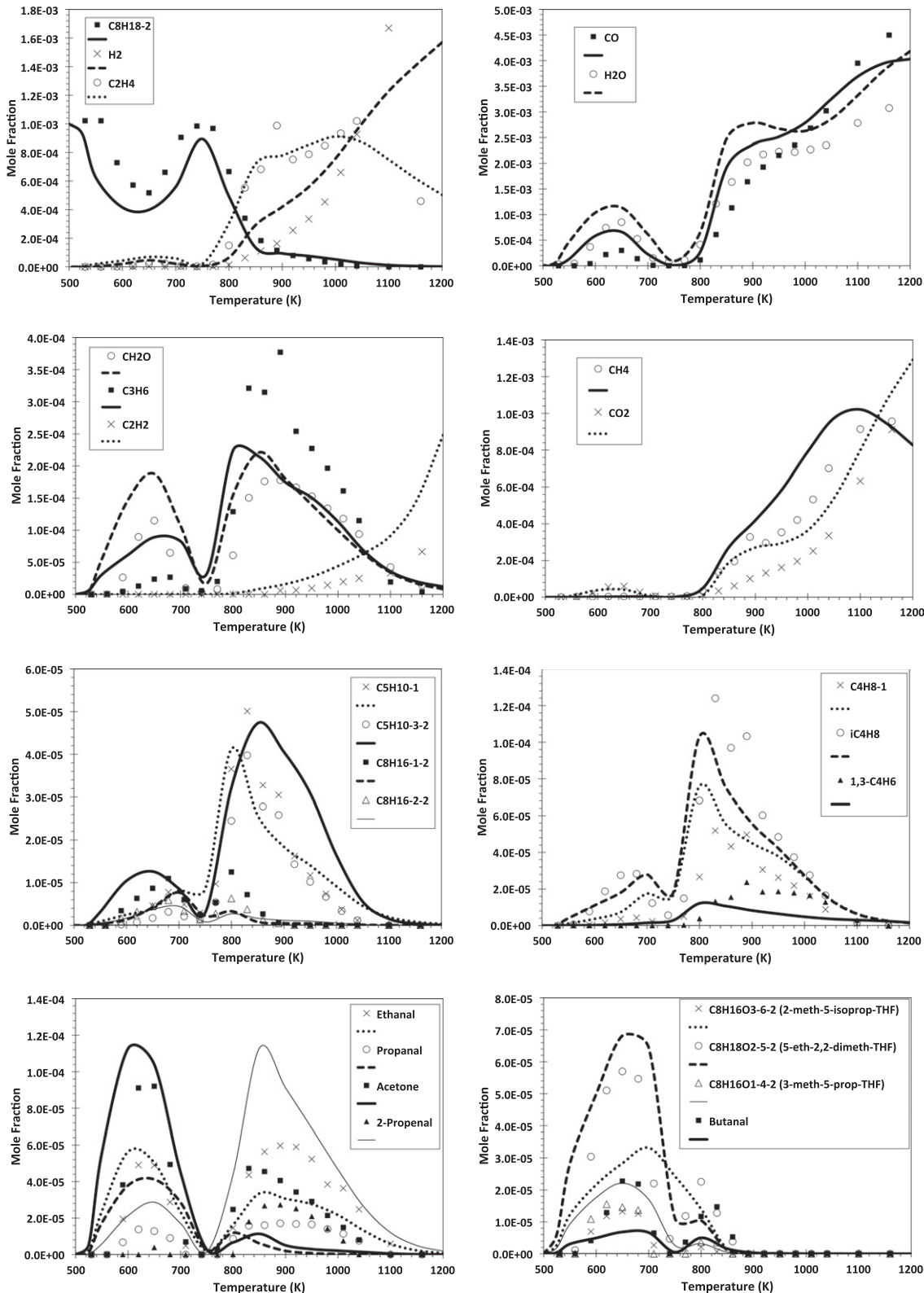


Fig. 5. 2-Methylheptane oxidation in a JSR at 10 atm, $\tau = 0.7$ s and $\phi = 2.0$. The initial fuel ($C_8H_{18}-2$) mole fraction was 0.1%. Experimental data (symbols) are compared to calculations (lines).

for low-temperature experiments with long ignition delay times (greater than approximately 1.5 ms), tailored N_2/He driver gas mixtures were used [68]. For all other experiments, helium was used as the driver gas. Post-shock conditions were determined

using the normal shock relations, known initial conditions, and measurement of the incident shock velocity made with a series of five pressure transducers located over the last meter of the driven section. The estimated uncertainty in the initial reflected shock

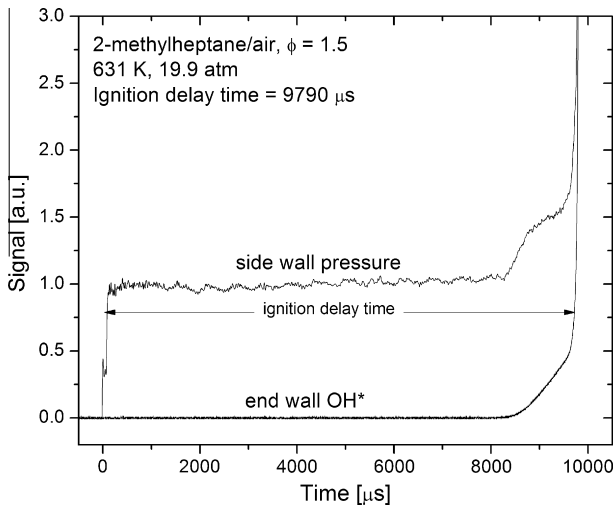


Fig. 6. Example ignition delay time measurement.

conditions is $\pm 1.5\%$ in temperature and $\pm 2.0\%$ in pressure (90% confidence interval), with the primary contribution due to the uncertainty in measured incident shock velocity. Due to non-ideal gas dynamic interactions, pressure and temperature rise with time in all reflected shock experiments. In the experiments reported here the measured pressure gradient was $dP/dt = 1\text{--}3\%\text{/ms}$. Assuming an isentropic relation between pressure and temperature this results in a temperature gradient of $dT/dt = 0.3\text{--}0.8\%\text{/ms}$.

Ignition delay times were measured using both pressure and electronically-excited OH (OH^*) chemiluminescence. Pressure was measured at a location 2 cm from the driven section end wall using a Kistler piezoelectric pressure transducer flush mounted in the driven section side wall. OH^* chemiluminescence was measured through a fused silica optic located in the driven section end wall using a high-speed silicon photo detector and a UG5 Schott glass filter. The ignition delay time was defined as the time interval between shock arrival and reflection at the end wall (time-zero) and the onset of ignition at the end wall. Time-zero was determined using measurement of the time of shock passage at a pressure transducer located 2 cm from the end wall and the measured incident shock velocity and the onset of ignition at the end wall was defined by extrapolating the maximum slope in OH^*

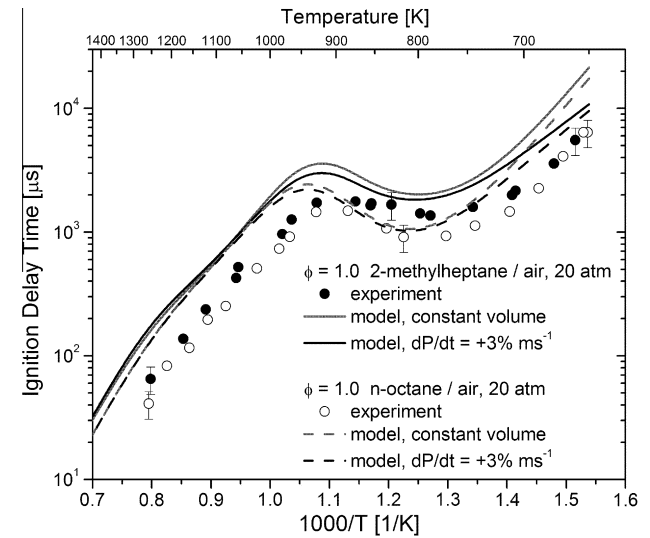


Fig. 8. Comparison of measured shock tube ignition delay times with kinetic modeling predictions for 2-methylheptane and *n*-octane at 20 atm in air. Kinetic modeling predictions are shown under the adiabatic constant volume constraint and for an imposed pressure rise rate of $dP/dt = 3\%\text{/ms}$, as experimentally measured.

emission to the baseline. See Fig. 6 for an example ignition delay time measurement for the experiment with the longest reported ignition delay time. The example in Fig. 6 illustrates a well behaved (relatively flat) pressure profile prior to energy release and a two-stage autoignition, characteristic of low-temperature alkane kinetics and observed previously in shock tube experiments for *n*-heptane [69] and *n*-decane [70]. The estimated uncertainty in ignition delay times is $\pm 25\%$ (90% confidence interval), which accounts for contributions from uncertainties in reflected shock temperature and pressure, fuel/air mixture composition, and determining ignition delay times from measured signals.

3.3.2. Shock tube autoignition results

Ignition delay time measurements are reported in the Supplementary material and shown in Figs. 7 and 8 with comparisons to kinetic modeling. The results for both 2-methylheptane and *n*-octane exhibit negative-temperature-coefficient (NTC) behavior

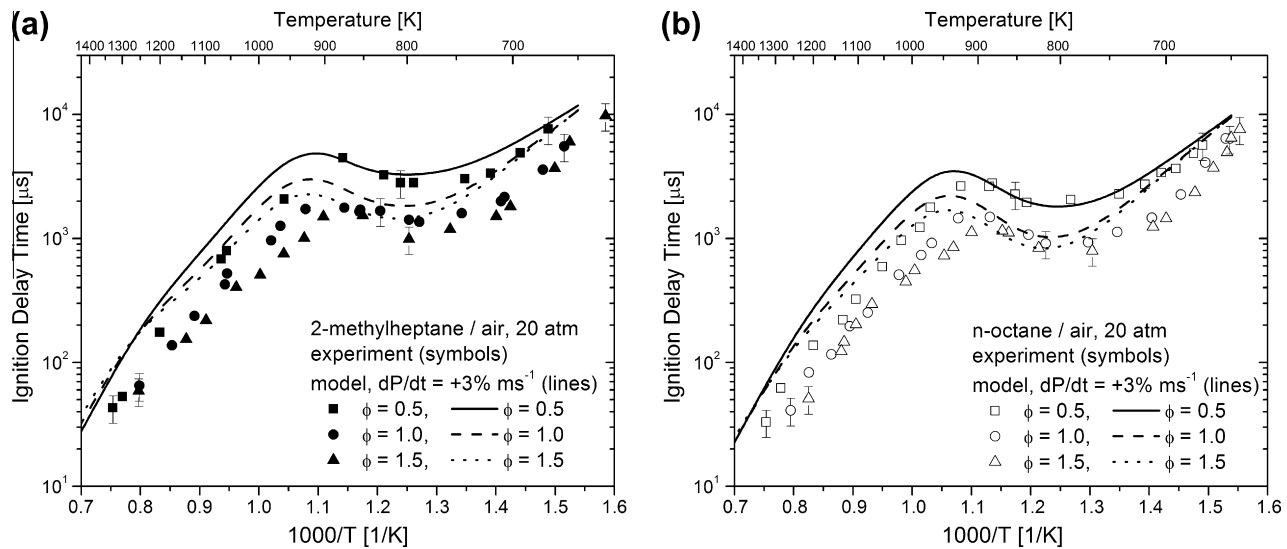


Fig. 7. Measured shock tube ignition delay times with comparison to kinetic modeling predictions: 2-methylheptane (left) and *n*-octane (right).

characteristic of alkanes and decreasing ignition time with increasing equivalence ratio. Comparison of the data for the two C₈ isomers illustrates the influence of the single methyl substitution in 2-methylheptane, which slightly reduces reactivity, particularly in the NTC regime, consistent with the general understanding of the influence of branching on aliphatic oxidation. At high temperatures ($T > 1000$ K) and low temperatures ($T < 750$ K) the differences between 2-methylheptane and *n*-octane ignition delay are relatively small (0–30%), within the $\pm 25\%$ uncertainty limits in ignition delay. On the other hand, in the NTC regime ($750 \text{ K} < T < 900$ K) the differences are somewhat larger, with 2-methylheptane having up to a factor of ~ 1.5 longer ignition delay time compared to *n*-octane at 800 K. While the difference of a factor of 1.5 in 2-methylheptane and *n*-octane ignition delay is approximately at the boundary of twice the $\pm 25\%$ uncertainty limits in absolute ignition delay, it should be noted that the largest portion of the absolute uncertainty is systematic uncertainty due to uncertainty in reflected shock temperature which should affect both *n*-octane and 2-methylheptane experiments equally, lending more confidence to the observed reactivity differences for these two compounds in the NTC.

The proposed chemical kinetic model was validated against the shock tube ignition data using the homogenous batch reactor code in CHEMKIN PRO [62]. Simulations of the shock tube test environment included a 3%/ms pressure rise rate, which was imposed by providing a calculated volume history, as described by Chaos and Dryer [71]. Simulations with the imposed positive 3%/ms pressure rate are compared to simulations performed using the adiabatic constant volume constraint (no pressure rise) in Fig. 8. The inclusion of the pressure rise has no influence on the simulations for temperatures greater than 1000 K. For temperatures from 700 to 1000 K the pressure rise results in a slight decrease ($\sim 25\%$) in simulated ignition delay. Only at the lowest temperatures studied (~ 650 K) does the pressure rise have a significant influence on simulated ignition delay (factor of two reduction).

Comparisons between experiment and kinetic model predictions illustrate that the model captures many of the experimental trends, including the difference in ignition delay for 2-methylheptane and *n*-octane in the NTC region. A later section of this paper uses the proposed kinetic model to rationalize the reduced reactivity of 2-methylheptane. The equivalence ratio dependence is also well captured by the model, but that modeling predictions for ignition delay are generally longer than experimental results for both compounds. At $\phi = 0.5$ the deviations between model and experiment range from within the experimental uncertainty in ignition delay ($\pm 25\%$) to a factor of two. At $\phi = 1.0$ and 1.5 the deviations in model and experiment are slightly larger and range from within the experimental uncertainty to a factor of three. This level of deviation between shock tube ignition delay and kinetic modeling is typical of *a priori* modeling comparison with no tuning of reaction rate coefficients and is simply due to the large number of chemical reactions required to model the oxidation of hydrocarbon compounds found in liquid transportation fuels and uncertainties in both the selection of reaction pathways and prescription/estimation of reaction rate coefficients. The deviations in model and experiment appear to be primarily due to differences in the predicted and observed transition from high-temperature Arrhenius behavior with positive activation energy to NTC behavior and the transition from NTC to low-temperature behavior, where positive overall activation energy is again established. The turnover from high-temperature to NTC behavior is experimentally observed to occur around 900 K but predicted by the model to occur at 950 K. The transition from NTC to low-temperature behavior is observed to occur around 770 K but predicted to occur around 800 K. These differences in the predicted and observed temperature dependencies are relatively small (4–6% deviations in the two trans-

sition temperatures described above). Improvement to modeling predictions will require examination of the reactions responsible for the transitions in oxidation regimes, namely the overall peroxy reaction sequence, $R + O_2 \leftrightarrow RO_2 \leftrightarrow QOOH(+O_2) \leftrightarrow OOQOOH \leftrightarrow 2OH + \text{products}$, including the inhibitive direct (i.e., concerted) HO₂ elimination and QOOH decomposition routes.

3.4. Laminar flame speed experiments and simulations of *n*-octane and 2-methylheptane

3.4.1. Laminar flame speed experimental setup

Laminar flame speed, S_u^0 , experiments were carried out for 2-methylheptane at the University of Southern California in the counterflow configuration at atmospheric pressure and an unburned reactant temperature of 353 K. Details of the experimental configuration and the fuel vaporization system have been described extensively in previous studies by the authors [72–76]. In order to determine S_u^0 the symmetric twin-flame configuration was used. The flow was seeded with 0.3 μm diameter silicon oil droplets, and the axial flow velocities were measured along the stagnation streamline using digital particle image velocimetry.

In order to determine S_u^0 , the minimum point of the axial velocity profile just upstream of the flame is measured and defined as the reference velocity, $S_{u,\text{ref}}$, and the absolute value of the maximum velocity gradient in the hydrodynamic zone is defined as the imposed strain rate, K , [75]. S_u^0 is subsequently determined through non-linear extrapolation of $S_{u,\text{ref}}$ to $K = 0$, using a computationally-assisted approach [74,76]. The standard deviation (2σ) in the determination of S_u^0 was quantified and is indicated with the appropriate bars in all figures. In general, the uncertainties in $S_{u,\text{ref}}$ for fuel-rich flames are larger than those of lean and near-stoichiometric flames. The uncertainty in ϕ is no larger than 0.5%.

3.4.2. Laminar flame speed results of 2-methylheptane and *n*-octane

Figure 9 depicts both experimental data and numerical predictions for the S_u^0 of 2-methylheptane/air and *n*-octane/air flames; the experimental data for *n*-octane/air flames were taken from [57]. Laminar flame speeds of 2-methylheptane/air flames are consistently 3.5–5 cm/s lower than those of *n*-octane/air flames. This is expected, as it has previously established experimentally (e.g., [57,77–79]) that branching in the fuel molecular structure reduces reactivity and as a result S_u^0 .

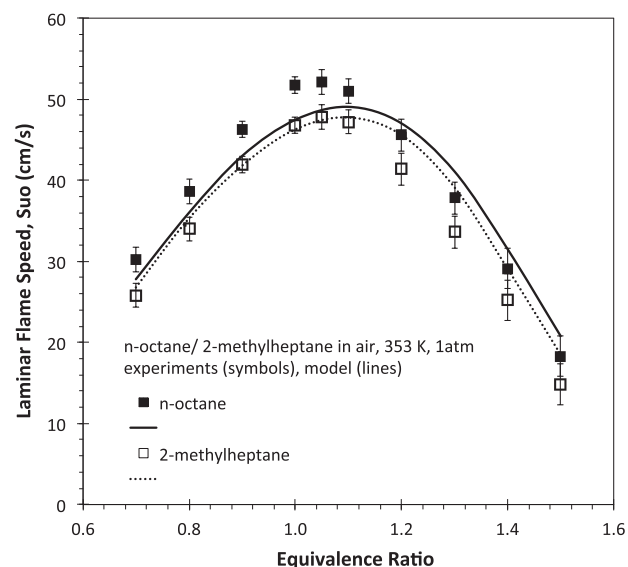


Fig. 9. Laminar flame speeds of *n*-octane (Ji et al. [57]) and 2-methylheptane in air at 353 K and 1 atm.

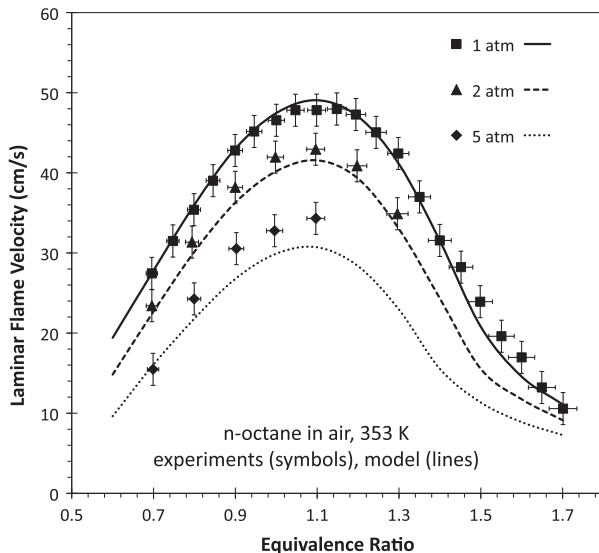


Fig. 10. Laminar flame speeds of *n*-octane (Kelley et al. [58]) at 353 K and various pressures.

Chemical kinetic modeling simulations of laminar flame speed were conducted using the PREMIX code in CHEMKIN PRO [62]. A high-temperature C₈ version of the detailed mechanism was used for these simulations, wherein species greater than C₈ and reaction classes 11–30 were removed. The resulting high temperature mechanism for 2-methylheptane consists of 714 species and 3397 elementary reaction steps. The simulations accounted for thermal diffusion, assumed mixture-averaged transport, and the solutions were highly resolved with approximately 200 grid points (GRAD 0.1, CURV 0.1). These calculated flame speeds were considered grid size independent when compared to several simulations run with 500 grid points (GRAD 0.05, CURV 0.05) that yielded maximum differences of less than 0.7 cm/s. The current model reproduces successfully the relative reactivities of these two fuels. The peak S_u^0 for both *n*-octane/air and 2-methylheptane/air flames occurs at $\phi \approx 1.05$. The predictions of the current model are in good agreement with the experimental data for 2-methylheptane flames for $0.70 \leq \phi \leq 1.10$. At higher ϕ 's, the model is over predicting the experimental results by approximately 4 cm/s. For *n*-octane/air flames, the agreement between the model and the experimental data taken from [57] are good for rich to stoichiometric conditions, and the model consistently under predicts the experimental results for fuel lean conditions. Figure 10 presents *n*-octane/air premixed laminar flame velocities at range of pressures [58] as an additional validation target for the proposed mechanism. The model exhibits excellent agreement with the experimental data at 1 atm and 2 atm. At 5 atm, the model under predicts the laminar flame velocity at equivalence ratios greater than 0.9.

In order to elucidate the reasons for lower flame speeds in 2-methylheptane compared to *n*-octane, a reaction flux analysis was conducted using PREMIX for both fuels at stoichiometric conditions and a temperature of approximately 1000 K. We do not present a figure of the flux analysis because the results are similar to those presented in a previous flame study by Sarathy et al. [28]. The results show that H-atom abstraction from the tertiary C–H site in 2-methylheptane followed by β -scission leads to the formation of iso-butene and subsequently the resonantly stabilized iso-but enyl radical. An analogous reaction sequence in *n*-octane leads to 1-butene and subsequently the 1-but enyl radical. In addition, the production of propene is greater in 2-methylheptane because the decomposition of most 2-methylalkyl radicals leads to propene (i.e., refer to flux diagram in [28]); propene then reacts to form

allyl. The increased stability of the iso-but enyl and allyl radicals is the reason for lower flame speeds in 2-methylheptane.

3.5. 2-Methylheptane model reduction and counterflow flame ignition and extinction

The previous validation studies all dealt with premixed reacting flows. However it is important to also validate the proposed model against non-premixed aerodynamically strained reacting flows because these conditions are often found in practical combustion applications. Flame extinction in strained flows is relevant to gas turbine engines, while flame ignition in strained flows is relevant to ignition in high swirl internal combustion engines. This section presents experimental data and simulated results for flame extinction and ignition in the counterflow configuration. Performing simulations of counterflow experiments with large chemical kinetic models is time consuming, highly demanding in computer memory requirements, and difficult to search for initial converged solutions. To minimize these difficulties, we reduced the size of the detailed chemical kinetic model.

3.5.1. Mechanism reduction

The reduced chemical kinetic mechanism for 2-methylheptane was created starting with the aforementioned high temperature C₈ detailed mechanism, which consists of 714 species and 3397 elementary reaction steps. The mechanism was reduced automatically using the method of directed relation graph (DRG) [80,81] to eliminate unimportant species and reactions for flame simulations. The DRG method quantifies species couplings as the pair-wise relative error induced to one species by the elimination of another. It then systematically identifies the species that are strongly coupled to the major species, such as the fuel, oxidizer, and important radicals, through a linear-time revised depth-first search (RDFS) method [82]. In a recent study [81], the DRG method was further improved by redefining the pair-wise relative error to species A induced by the elimination of species B as:

$$r_{AB} = \frac{\max_i |\nu_{A,i} \omega_i \sigma_{Bi}|}{\max_i |\nu_{A,i} \omega_i|}, \quad \sigma_{Bi} = \begin{cases} 1, & \text{if the } i\text{th reaction involves } B \\ 0, & \text{otherwise} \end{cases} \quad (1)$$

where ω_i is the net reaction rate of the i th reaction and $\nu_{A,i}$ is the stoichiometric coefficient of species A in the i th reaction. It was shown in Ref. [81] that the definition of r_{AB} in Eq. (1) is more advantageous than that in the original DRG method [80] when the detailed mechanism consists of a large number of isomers, e.g., that in the present mechanism for 2-methylheptane and other engine fuels with long chains.

The reduction was performed based on reaction states sampled in a parameter range that is relevant to the ignition and extinction of the counterflow flames in the present work. The reaction states for ignition study were sampled from auto-ignition calculated with SENKIN [83], and reaction states for extinction were sampled from perfectly stirred reactors (PSR) [84]. Both applications were simulated under atmospheric pressure for 2-methylheptane–air mixtures with equivalence ratios between 0.5 and 2.0. The initial temperature for ignition was set to be 1000–1800 K. The inlet temperature for PSR was fixed at 300 K, which gave reactor temperatures of 1000–2300 K for 1 atm and the stoichiometry considered. These temperature ranges were chosen to cover the temperature ranges expected in the extinction and ignition experiments in the counterflow apparatus.

It is noted that although the non-premixed counterflow flames may involve mixtures with arbitrary equivalence ratios, previous studies indicate that mechanisms reduced in the above range of

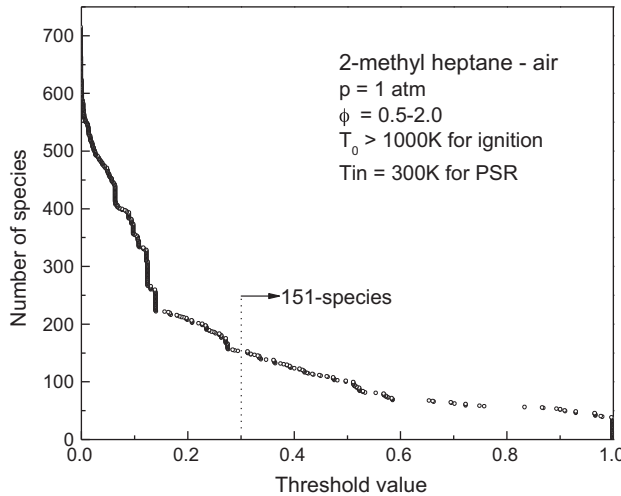


Fig. 11. The reduction curve of DRG using the definition in Eq. (1) for 2-methylheptane-air mixtures based on reaction states sampled from auto-ignition and PSR.

equivalence ratio are typically applicable to non-premixed flames in predicting such phenomena as ignition and extinction [85]. This is primarily because the reaction zone of a non-premixed flame tends to be located near the stoichiometric surface, and mixtures far away from the reaction zone are typically dominated by the transport processes rather than chemistry. It is further noted that the ignition of high strain rate, low fuel mass fraction counterflow flames, similar to the one studied here, are insensitive to low-temperature chemistry [80,86,87]. Therefore the present reduced mechanism developed for high temperatures (above 1000 K) is adequate for the counterflow ignition study in the present work, while it should not be applied where low-T chemistry is important (e.g., oxidation in JSR, ignition in RCM and homogeneous charge compression ignition (HCCI) engines, or counterflow flames at low strain rates and high fuel mass fraction).

The number of species in the skeletal mechanism as a function of the threshold value, ε , to truncate the r_{AB} values in Eq. (1) based on the sampled reaction states is shown in Fig. 11. By specifying a critical value of $\varepsilon = 0.3$, which is roughly equivalent to the worst-case relative error of about 23% based on the definition of r_{AB} in the original DRG method [80], a skeletal mechanism with 151 species and 989 reactions was obtained. While further reduction can be achieved either by further increasing the error threshold or by employing other reduction methods such as DRG aided sensitivity analysis (DRGASA) [87,88], the 151-species skeletal mechanism was selected to simulate the counterflow flames in the present work considering that such a mechanism size is affordable for the present simulations and it is important to avoid unnecessary loss in chemical fidelity for the analysis of detailed reaction pathways.

For mechanism validation, Fig. 12 shows the temperature profiles for adiabatic PSR and auto-ignition within the parameter range of the reduction, calculated with the 151-species and the detailed high temperature C₈ mechanisms, respectively. It is seen that the skeletal mechanism agrees closely with the detailed mechanism, with a worst-case error of approximately 20% observed in the extinction time of the PSR, which is the residence time at the turning point on the temperature profile. It is further seen that the skeletal mechanism not only accurately predicts the global parameters of PSR extinction times as shown in Fig. 13a and ignition delay times for auto-ignition as shown in Fig. 13b, c, and d, but also reproduces the detailed structures of the temperature profiles. This implies that the important species and reaction pathways were correctly retained in the reduction for various stages of the

oxidation. In the following, the mechanism will be employed to predict ignition and extinction of 1-D counterflow diffusion flames.

3.5.2. Counterflow flame experimental setup

Extinction and auto-ignition of non-premixed flames of 2-methylheptane were measured employing the counterflow configuration. Figure 13 shows a schematic illustration of the counterflow configuration. Steady, axisymmetric, laminar flow of two counterflowing streams toward a stagnation plane is considered. In this configuration, a fuel stream made up of prevaporized 2-methylheptane and nitrogen is introduced through the bottom duct, and an oxidizer stream of air is injected through the upper duct. A mixing-layer develops around the stagnation plane. The exit of the fuel duct is called the fuel boundary and the exit of the oxidizer duct the oxidizer boundary. Fine wire screens are located at the exits of the ducts. As a consequence, the tangential component of the flow velocities vanishes at the boundaries. This allows the use of “plug flow boundary conditions” in numerical simulations. The mass fraction of fuel, temperature, and the component of the flow velocity normal to the stagnation plane at the fuel boundary are represented by $Y_{F,1}$, T_1 , and V_1 , respectively. The mass fraction of oxygen, temperature, and the component of the flow velocity normal to the stagnation plane at the oxidizer boundary are represented by $Y_{O2,2}$, T_2 , and V_2 , respectively. The exit diameter of the fuel duct and the oxidizer duct is 23 mm. L represents the distance between the fuel boundary and the oxidizer boundary. The value of the strain rate, defined as the normal gradient of the normal component of the flow velocity, changes from the fuel boundary to the oxidizer boundary. For the experimental conditions considered, the flame is located on the oxidizer side of the stagnation plane where the characteristic strain rate, a_2 , is given by Eq. (2) [89],

$$a_2 = \frac{2|V_2|}{L} \left(1 + \frac{|V_1|\sqrt{\rho_1}}{|V_2|\sqrt{\rho_2}} \right) \quad (2)$$

Extinction experiments were conducted with a duct separation of $L = 10$ mm, and $T_2 = 298$ K. The temperature of the fuel stream, T_1 , for all fuels is 400 K. At some selected value of $Y_{F,1}$, the flame was stabilized. The strain rate was increased by increasing V_1 and V_2 simultaneously, keeping momenta of the counterflowing streams balanced based on $\rho_1 V_1^2 = \rho_2 V_2^2$ until extinction was observed.

Auto-ignition experiments were carried out with a duct separation of $L = 12$ mm, a fuel stream temperature of 400 K (± 5 K) and a fuel mass fraction, $Y_{F,1} = 0.4$. For selected values of strain rate a_2 the oxidizer stream temperature was increased until auto-ignition took place. The velocities of the counterflowing streams were constantly adjusted based on the change in temperature to satisfy the momentum balance equation.

The accuracies of the strain rate and fuel mass fraction were 5% and 3% of the recorded values, respectively. The experimental repeatability of the reported strain rate at extinction was 3% of recorded value. The accuracy of the measurement of the oxidizer temperature was determined to be ± 20 K. The experimental repeatability on recorded temperature of air at auto-ignition was ± 5 K.

3.5.3. 2-Methylheptane counterflow flame ignition and extinction results

The skeletal mechanism was used to compute critical conditions of extinction and ignition, and the results were compared to the experiments. The extinction computations were carried out using extinction solver in CHEMKIN PRO [62], which uses the arc length continuation method to generate the S-shaped response curve [90,91]. Plug flow boundary conditions were employed in the

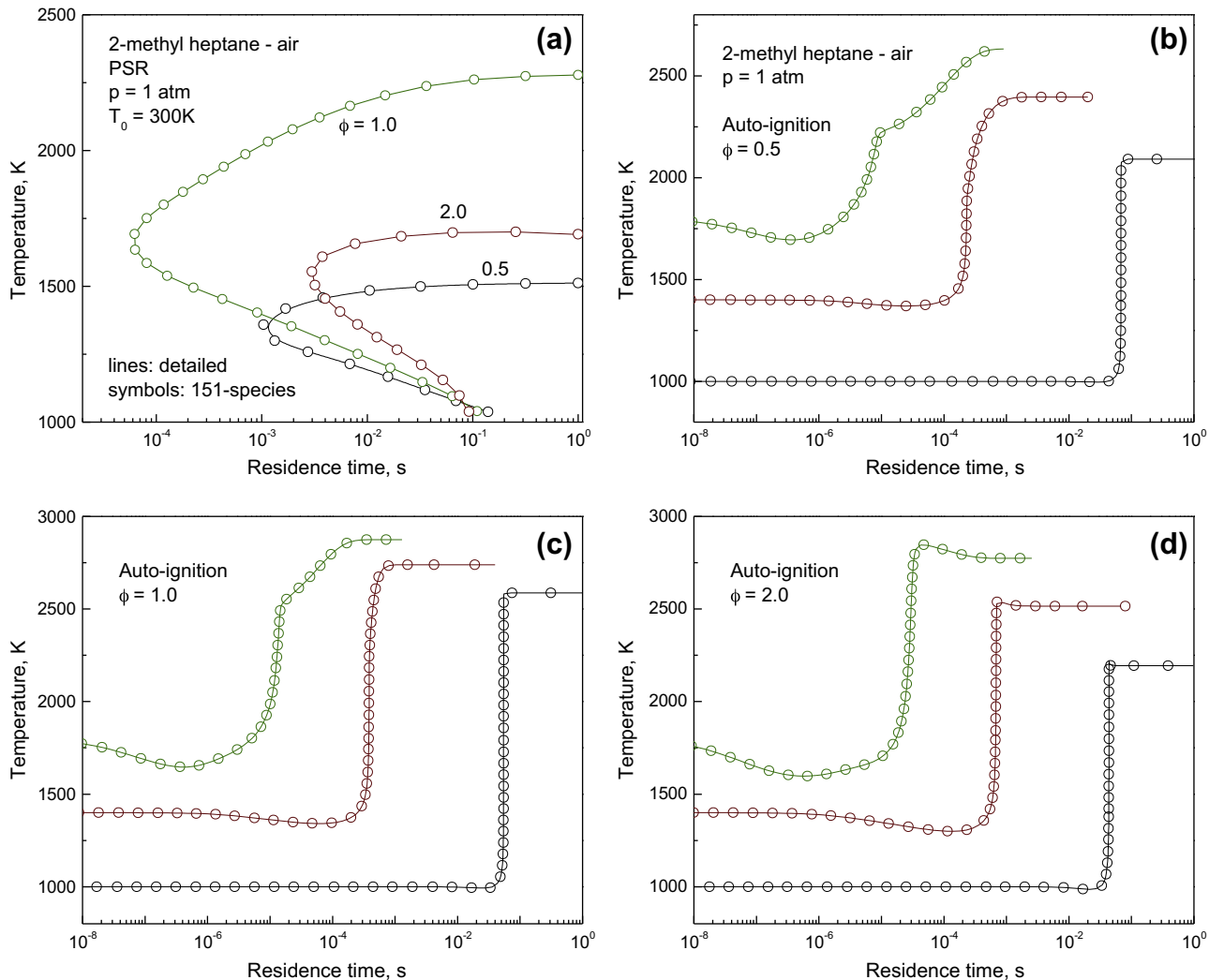


Fig. 12. Temperature as a function of the residence time calculated using the 151-species skeletal mechanism and the detailed high temperature C₈ mechanism, respectively, for 2-methylheptane-air mixtures under atmospheric pressure for PSR and different inlet temperatures for auto-ignition.

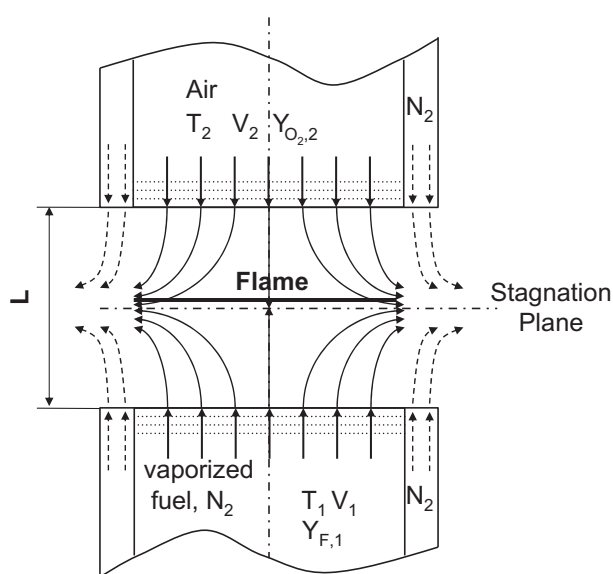


Fig. 13. Schematic illustration of the counterflow flow field.

calculations. For a given composition and temperature of the reactant streams at the boundaries, the flow velocities V_1 and V_2 were increased until extinction takes place. The strain rate at extinction is calculated using Eq. (2). The 1-point extinction method was employed with mixture-averaged transport and no thermal diffusion (GRAD 0.1, CURV 0.3). If the 1-point extinction method failed, then the 2-point method was used. We were unable to obtain a converged solution using thermal diffusion or using the more accurate yet computationally expensive multi-component transport model.

Ignition calculations were performed using the OPPDIF solver in CHEMKIN PRO using the following procedure. We made an initial guess for the temperature profile and computed a fully resolved, cold solution temperature profile. Then we used the cold solution temperature profile as an initial guess and iteratively increased the temperature of air at the boundary, T_2 , in the simulations until ignition took place. The composition of the reactant streams, their inlet flow velocities and the value of the fuel stream temperature, T_1 , were all maintained constant during this procedure. The strain rate at ignition was calculated using Eq. (2). The simulation employed mixture-averaged transport and thermal diffusion (GRAD 0.1, CURV 0.2).

Figure 14 shows the mass fraction of fuel, $Y_{F,1}$, as a function of the strain rate at extinction, $a_{2,e}$. The symbols in this figure represent experimental data and the line represents the calculations.

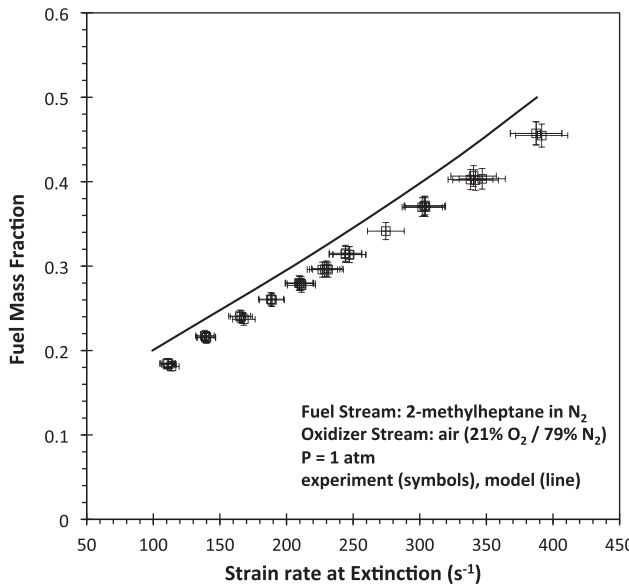


Fig. 14. The mass fraction of fuel, $Y_{F,1}$, as a function of the strain rate at extinction, $a_{2,e}$ in the counterflow flame. The symbols represent experimental data. The line is results of numerical calculation using the skeletal mechanism.

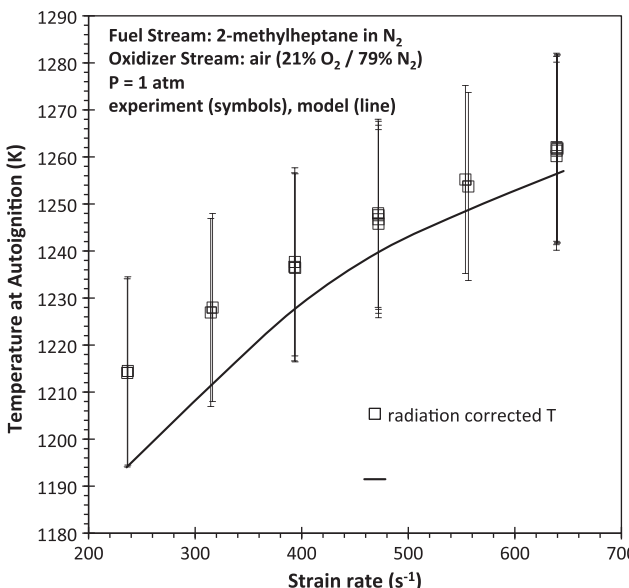


Fig. 15. The temperature of the oxidizer stream at ignition, $T_{2,l}$, as a function of the strain rate, a_2 for $Y_{F,1} = 0.4$ in the counterflow flame. The symbols represent experimental data. The line is result of numerical calculations using the skeletal mechanism.

Multiple symbols give an indication of reproducibility of the experiments at a targeted condition. They separate a flammable region for $a_2 < a_{2,e}$ from a nonflammable region for $a_2 > a_{2,e}$. At a given value of strain rate the calculated fuel mass fraction at extinction is slightly higher than the measured value, but the overall agreement is considered reasonably good for these types of experiments. Figure 15 shows the temperature of air at ignition, $T_{2,l}$, as a function of the strain rate, a_2 , for values of $Y_{F,1} = 0.4$. The symbols represent experimental data with radiation corrected temperatures presented. Again, multiple symbols give an indication of reproducibility of the experiments at a targeted condition. The line represents results of numerical calculations using the skeletal mechanism. It separates a region for $T_2 > T_{2,l}$ where ignition can take place from

a region where ignition is not possible. For a given a_2 , the calculated value of $T_{2,l}$ is lower than the measured temperature corrected for radiation losses. Considering the error on the temperature measurements is ± 20 K, the model predictions are considered to be excellent.

It should be noted that the counterflow flame predictions are sensitive to the transport parameters used to calculate fuel diffusivity in the flame. In a previous study, we [28] showed that decreasing the collision diameter of 2-methylheptane (i.e., increasing fuel diffusivity) has a significant impact on predicted species profiles in counterflow diffusion flames. Holley et al. [49] have shown that increasing the binary diffusivity of fuel-N₂ in *n*-alkane counterflow flames increases the resistance to non-premixed counterflow extinction. Smallbone et al. [92] have shown a decrease in non-premixed counterflow autoignition temperatures when the binary diffusivity of *n*-heptane-N₂ increases.

4. Modeling predictions

4.1. Kinetic modeling simulations of shock tube ignition delay time for *n*-alkanes and 2-methylalkanes greater than C_8

In a previous study on *n*-alkanes [2], we presented kinetic modeling simulations of shock tube ignition delay time for *n*-alkanes from *n*-heptane (i.e., C_7) through *n*-hexadecane (i.e., C_{16}) at 13.5 bar initial pressure and stoichiometric conditions. The simulations at these conditions indicated that each fuel compound has virtually identical ignition delay times with only a slight trend in the NTC region of faster ignition delay times as the carbon chain length increases (i.e., increasing reactivity with increasing carbon number). The aforementioned results are surprising because one would expect ignition delay times to be observably different for long chained alkanes. Biet et al. [93] also simulated ignition delay times of *n*-alkanes at 12 bar initial pressure and stoichiometric conditions; and showed that increasing the chain length slightly decreases ignition delay times at all temperatures.

In order to better understand the effects of carbon chain length on auto ignition properties of *n*-alkanes and 2-methylalkanes, we conducted kinetic modeling simulations of shock tube ignition delay for even carbon number fuel compounds from C_8 to C_{16} . Since these compounds are important diesel fuel constituents, we conducted simulations at conditions that are relevant for diesel combustion applications. A phenomenological study of diesel combustion by Dec [94] indicates that auto ignition occurs in a fuel-rich zone downstream of the penetrating liquid jet. An equivalence ratio of 2–4 exists in this zone and in-cylinder pressures are in the region of 50 atm. This suggests that shock tube simulations at 12–13 bar initial pressure and stoichiometric conditions do not well represent the conditions under which diesel fuel ignition occurs in engines. Therefore, we conducted simulations at initial pressures of 20 atm and rich equivalence ratios (i.e., $\phi = 3$) because these conditions are more relevant to practical applications.

Figure 16 presents the simulated ignition delay times for even carbon number *n*-alkanes from C_8 to C_{16} and 2-methylalkanes from C_8 to C_{20} . The previous shock tube experimental and modeling section showed that *n*-octane exhibits faster ignition delay times than 2-methylheptane in the NTC region; a similar decrease in reactivity is observed for larger 2-methylalkanes when compared to *n*-alkanes of the same chain length. This trend agrees well with the lower DCN values measured for 2-methylalkanes compared to *n*-alkanes of the same chain length (e.g., refer to Table 1). The simulations also indicate an observable decrease in ignition delay time as the size of the carbon chain increases from C_8 to C_{10} to C_{12} . However, *n*-tetradecane (C_{14}) and *n*-hexadecane (C_{16}) exhibit more similar reactivity at all temperatures, which suggests that the adding

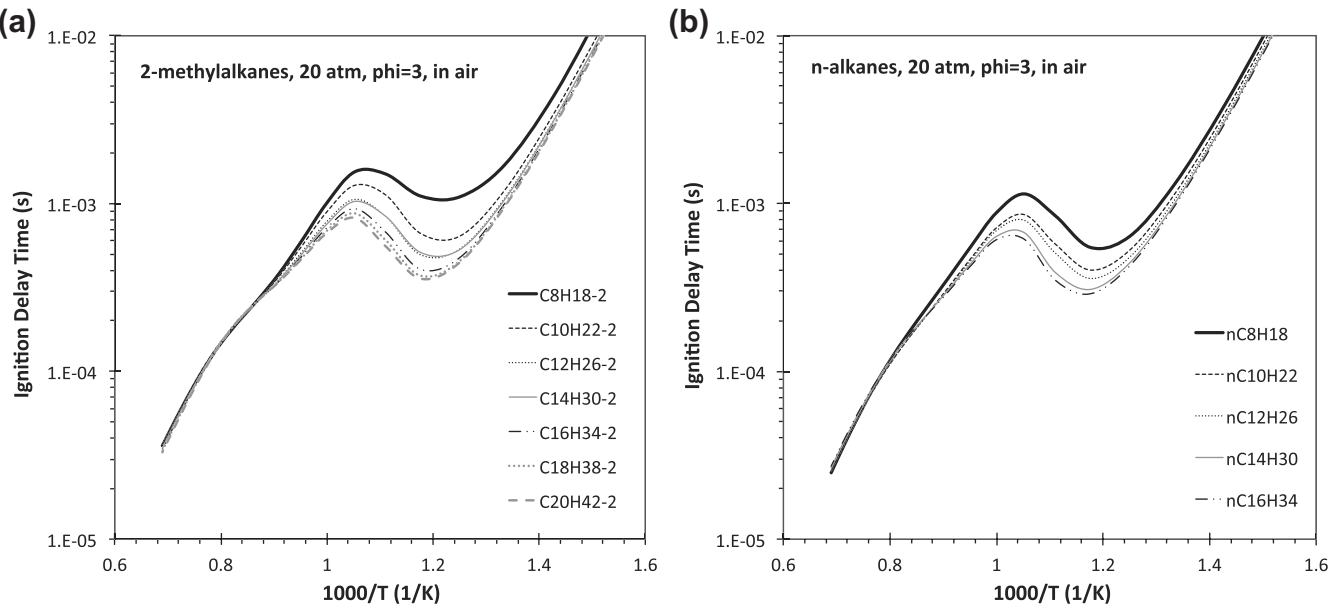


Fig. 16. Computed ignition delay times for even carbon number *n*-alkanes and 2-methylalkanes from C_8 to C_{16} at 20 atm, $\phi = 3$, in air.

carbon atoms does not increase reactivity after the carbon chain reaches a critical length. A similar diminishing returns is observed for the 2-methylalkanes, wherein 2-methylheptadecane (C_{18}) and 2-methylnonadecane (C_{20}) all exhibit similar reactivity. These simulated observations are generally consistent with experimentally measured cetane numbers that indicate a large increase in cetane number from *n*-octane (C_8 CN = 65) to *n*-tetradecane (C_{14} CN = 96), followed by much smaller increases as the carbon chain length increases above C_{14} (e.g., C_{16} CN = 100, C_{18} CN = 110, C_{20} CN = 110) [95]. Although kinetic effects play a role in diesel engine ignition delay (i.e., cetane number rating), the physical effects (e.g., density, viscosity, vapor pressure) on spray combustion are also important factors to consider. Therefore, the conclusions drawn here from kinetic modeling simulations should be considered in conjunction with physical contributions of chain length on a fuel's cetane number. Further experimental studies of large 2-methylalkanes in idealized combustion systems (e.g., shock tubes and rapid compression machines) are needed to confirm whether or not the simulated predictions agree with the behavior of real systems.

We can use the proposed chemical kinetic model to elucidate why 2-methylalkanes exhibit longer ignition delay times in the NTC region (i.e., decreased low temperature reactivity) compared to *n*-alkanes. The observed differences are due to a number of factors, which can all be directly related to the presence of a tertiary carbon (i.e., methyl branch) in the 2-methylalkanes.

Figure 17 displays a comparison of low temperature chain branching pathways for 2-methylheptane and *n*-octane, which are important in controlling reactivity at temperatures below approximately 750 K. It is shown that H-atom abstraction from the secondary carbon (i.e., #2 carbon) in *n*-octane leads to a radical, to which O_2 is subsequently added. The resulting ROO radical then undergoes a rapid six-member ring internal isomerization to form a QOOH radical. Another O_2 is added to the molecule, and the resulting O_2 QOOH radical undergoes a second internal isomerization to abstract an H-atom from the carbon bonded to the OOH moiety, since this carbon bond has a lower C-H bond strength than a normal C-H bond and makes it easier to abstract. This second six-member isomerization has a reaction rate constant that is the same as the first six-member isomerization (i.e., $ROO=QOOH$), except the activation energy is 3 kcal/mol lower to account for the weakened C-H bond. The resulting radical then rapidly decomposes to

form an OH radical and a ketohydroperoxide, which subsequently decomposes to an OH radical and smaller oxygenated species; thus, the low temperature chain branching process is completed. The analogous reaction pathways for 2-methylheptane indicate why it exhibits less low temperature reactivity. H-atom abstraction from the tertiary carbon (i.e., #2 carbon) in 2-methylheptane initiates a similar reaction sequence as shown previously. However, the second isomerization is noticeably different in 2-methylheptane because there are no free C-H bonds on the carbon atom bonded to the OOH moiety. As a result, the second six-member isomerization abstracts an H-atom from a secondary carbon atom (i.e., #4 carbon) at a rate identical to the first six-member isomerization. The subsequent radical then continues onward to produce OH radicals and smaller oxygenated species similar to the *n*-octane system. The overall reactivity of 2-methylheptane is lower because the second isomerization proceeds at a slower rate than the analogous reaction in *n*-octane.

We have shown how the tertiary carbon leads to less low temperature reactivity, but the presence of the methyl branch also affects the carbons surrounding it. The increase in the number of primary carbon atoms limits chain branching by introducing strong primary C-H bonds that are difficult to break during internal isomerization. For example, when O_2 adds to a radical site on the #3 carbon, the resulting ROO radical now has two competing six-member internal isomerization pathways that involve strong primary C-H bonds; the analogous reaction in an *n*-alkane only has one competing primary C-H bond for competition. Additionally, when O_2 adds to a radical site on one of the primary carbons (i.e., #1 carbons), the resulting ROO radical has a competing six-member internal isomerization pathway that involves the other primary carbon atom; such a pathway does not exist in an *n*-alkane.

In total, we calculate that introducing methyl branch at the #2 location depresses the low temperature reactivity of three carbon atoms in the molecule. One would expect that as the size of a 2-methylalkane increases the inhibitory effects of the methyl branch decreases, and our simulations presented in Fig. 17 confirm this hypothesis. For C_8 molecules at 850 K, it is shown that 2-methylheptane has ignition delay approximately 2 times longer than *n*-octane. However, for C_{16} molecules at 850 K, it is shown that 2-methylpentadecane is only 1.4 times slower than *n*-hexadecane.

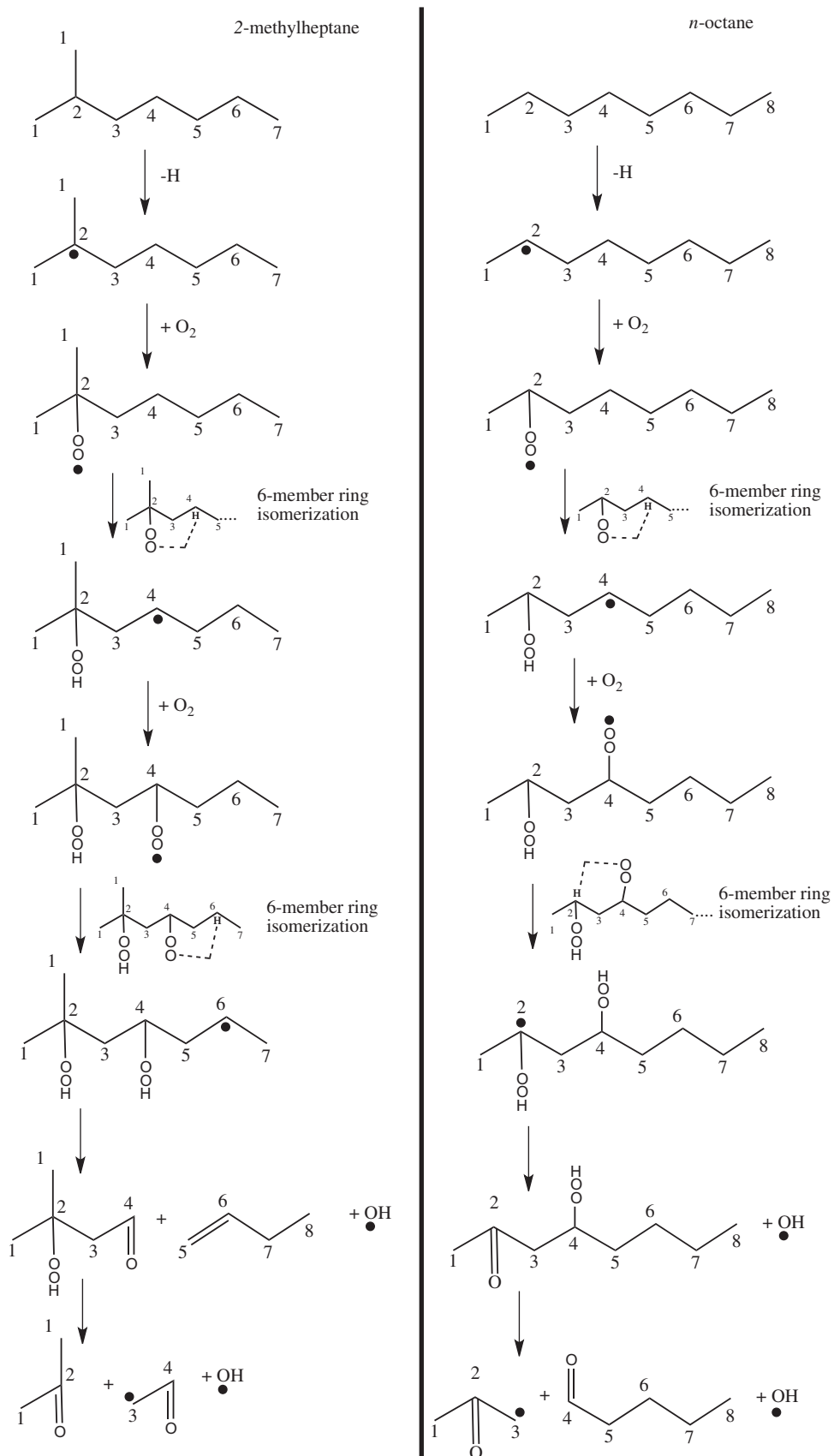


Fig. 17. Comparison of low temperature chain branching pathways for 2-methylheptane and *n*-octane.

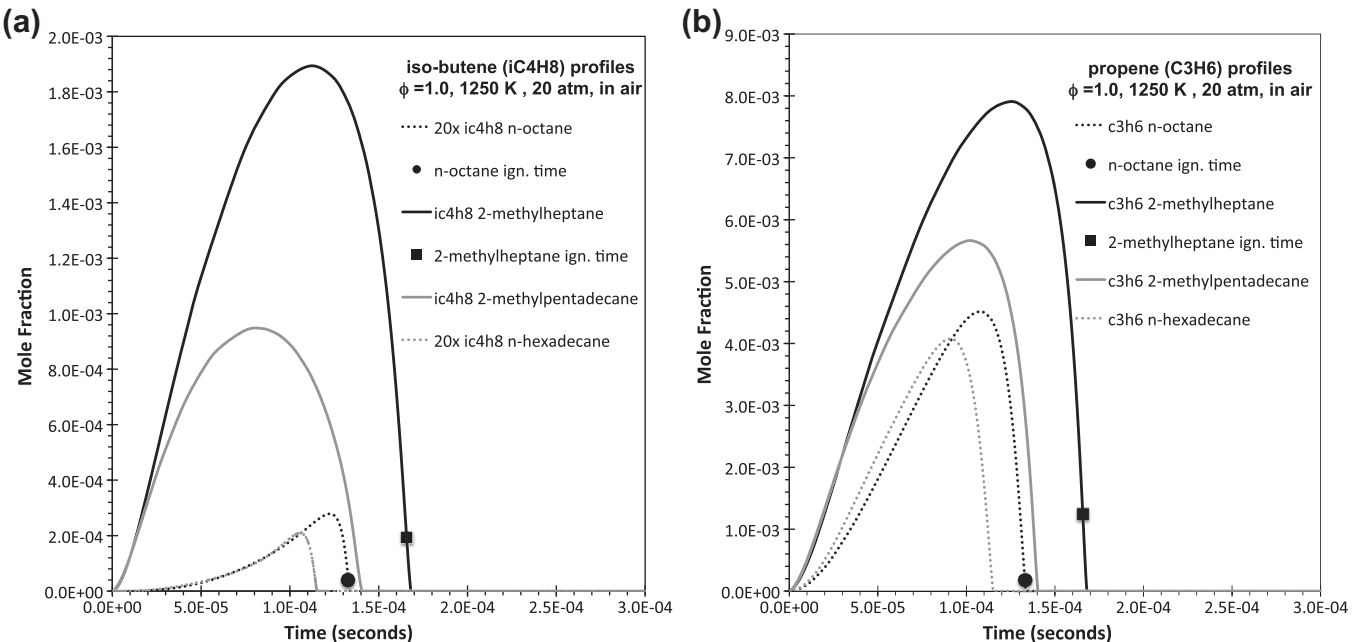


Fig. 18. Predicted species time histories of iso-butene and propene for 2-methylheptane, n-octane, 2-methylpentadecane, and n-hexadecane under constant volume shock tube conditions ($\phi = 1.0$, $P = 20$ atm, $T = 1250$ K). Note that iso-butene concentrations for n-alkanes are multiplied by 20×.

At high temperatures (e.g., above 1200 K) the model predicts longer ignition delay times for 2-methylalkanes compared to n-alkanes. In addition, experimental data points in Fig. 8 at 1250 K (i.e., $1000/T = 0.8$) also indicate that 2-methylheptane is less reactive than n-octane. Figure 18 displays iso-butene and propene species time histories at $\phi = 1.0$ and 1250 K for n-octane, 2-methylheptane, n-hexadecane, and 2-methylpentadecane. The results indicate that the 2-methylalkanes produce more iso-butene and propene than n-alkanes of the same chain length. This occurs because the weak tertiary C-H bond easily undergoes H-atom abstraction and then β-scission to form iso-butene. In addition, H-atom abstraction from most secondary C atoms leads to a radical that usually decomposes to form propene. Essentially, the methyl branch is preserved during combustion and this contributes to a greater production iso-butene and propene. This increased concentration of iso-butene and propene decreases system reactivity because radicals can easily abstract hydrogen atoms from the allylic sites and form the resonantly stabilized iso-butenyl (i.e., methyl allyl) and allyl radicals. Therefore, iso-butene and propene essentially behave as sinks for reactive radical species (e.g., H, OH, HO₂). It should be noted that this conclusion should not be extrapolated to higher temperatures where unimolecular decomposition reactions become increasingly important.

5. Conclusions and outlook

This study presented a comprehensive experimental and modeling study for the oxidation of 2-methylalkanes and n-alkanes larger than C₈. New experimental data was presented for 2-methylheptane in a jet stirred reactor, shock tube, premixed laminar flame, and counterflow diffusion flame. The detailed mechanism exhibited good agreement with the various sets of experimental data. A skeletal mechanism derived from the detailed mechanism well reproduced counterflow flame extinction and ignition experimental data.

Jet stirred reactor experiments and model predictions indicate that branched alkenes (i.e., 2-methylalkenes) are important intermediates in the oxidation of 2-methylheptane. The experimentally

observed cool flame reactivity, NTC behavior, and transition to high temperature oxidation are all well predicted by the proposed model. Transitions between chain branching peroxy chemistry, concerted elimination reactions, cyclic ether formation, and β-scission reactions are responsible controlling the overall reactivity of the 2-methylheptane oxidation system.

Both the experiments and model predictions indicate that 2-methylalkanes have longer shock tube ignition delay times than n-alkanes of the same chain length. Simulations conducted under diesel relevant conditions indicate that the reactivity of 2-methylalkanes and n-alkanes increase with increasing carbon number; however, a plateau in reactivity is eventually achieved. Experimental ignition data at high pressures and rich conditions are needed to verify these model predicted trends.

Premixed laminar flame speeds are slower for 2-methylheptane when compared to n-octane because of the increased production of the resonantly stabilized iso-butenyl and allyl radicals. The proposed model well reproduces these changes in flame speeds due to the adding of a methyl branch. The present study has also exhibited the potential of using computational techniques to reduce the detailed mechanism and well predict one-dimensional counterflow diffusion flame ignition and extinction data.

We have noted that very few experimental studies are available for validation of the present 2-methylalkane kinetic mechanisms. We hope that the existence of these mechanisms will encourage other experiments to test the model predictions and improve their accuracy and predictive capabilities. At the same time, we are confident that the systematic processes used to extend the mechanisms for 2-methylheptane to larger 2-methylalkane fuels indicate that the present mechanisms can provide considerable confidence in their ability to predict combustion behavior of this class of hydrocarbon fuels.

The present 2-methylalkane/n-alkane chemical kinetic mechanism has the potential of significantly improving our understanding of diesel and jet fuel combustion. The structures present within the mechanism can be used to develop surrogate fuel formulations for a wide variety of fuels, such as conventional petroleum derived fuels, synthetic Fischer-Tropsch fuels, and renewable fuels derived from thermochemical treatment of

bio-derived fats and oils (e.g., HRJ fuels). For example, previous studies that developed surrogate kinetic models for Jet-A [96] and F-T jet fuels (e.g., S-8) [97,98] only had the option of using a highly branched molecule, iso-octane, as the surrogate for the lightly branched alkanes found in real fuels because detailed kinetic models for latter were unavailable at the time. Therefore, the present study provides immediate potential of improving the chemical fidelity of surrogate fuel models.

In addition to improving surrogate fuel models, this study provides fundamental information on the effects of methyl branching. We aim to advance this understanding by determining the effects methyl branch location and number by extending the proposed mechanism to include other lightly branched alkanes (e.g., 3-methylalkanes and dimethylalkanes) that are also present in real fuels. The inclusion of these additional species will undoubtedly increase the size and complexity of our models. Therefore, we encourage and are actively pursuing the use of mechanism reduction techniques to decrease the size of the detailed mechanism, and thus enable their use in three-dimensional computational fluid dynamics (3D-CFD) engine-like simulations [99,100].

Acknowledgments

The authors thank National Renewable Energy Laboratory researchers Matthew Ratcliffe and Jon Luecke, as well as Gregory Bogin, Jr. from the Colorado School of Mines for providing unpublished derived cetane numbers for *n*-alkanes and 2-methylalkanes. The work at LLNL work was supported by the US Department of Energy, Office of Vehicle Technologies and the Office of Basic Energy Sciences, and the authors thank program managers Gurpreet Singh, Kevin Stork, and Wade Sisk. This work was performed under the auspices of the US Department of Energy by Lawrence Livermore National Laboratory under Contract DE-AC52-07NA27344. The research at the University of California at San Diego was supported by the US Army Research Office, Grant # W911NF-09-1-0108, Program Manager Dr. Ralph A. Anthenien, Jr. The work at University of Connecticut was supported by the National Science Foundation under Grant 0904771. The work at the University of Southern California was sponsored by the U.S. Air Force Office of Scientific Research AFOSR (Grants No. FA9550-10-1-0087 and FA9550-08-1-0040) under the technical supervision of Dr. Julian M. Tishkoff. The coauthor S.M.S. acknowledges fellowship support from the Natural Science and Engineering Research Council of Canada (NSERC).

Appendix A. Supplementary data

This publication includes the following supplemental material:

1. A complete description of the detailed chemical kinetic mechanism reaction pathways and reaction rate rules.
 2. Raw experimental data for shock tube ignition delay measurements of *n*-octane and 2-methylheptane.
 3. Raw experimental data for JSR data, laminar flame speed data, and counterflow extinction and ignition data (in EXCEL format).
 4. A supplementary figure displaying critical temperatures (T_c), boiling temperatures (T_b), and critical pressures (P_c) for 2-methylalkanes and the use of extrapolation with power law functions.
 5. A complete detailed chemical kinetic mechanism covering high and low temperature reactivity of *n*-alkanes up to C_{16} and 2-methylalkanes up to C_{20} in CHEMKIN format (.INP format).
 6. A detailed chemical kinetic mechanism covering high and low temperature reactivity of *n*-alkanes and 2-methylalkanes up to C_8 in CHEMKIN format (.INP format).
 7. A smaller detailed chemical kinetic mechanism covering high temperature reactivity of *n*-alkanes and 2-methylalkanes up to C_8 in CHEMKIN format (.INP format).
 8. A 151-species skeletal mechanism for 2-methylheptane generated using the DRG methodology (.INP format).
 9. The proposed thermodynamic datafile in CHEMKIN format (.DAT format).
 10. The proposed transport datafile in CHEMKIN format (.DAT format).
- Supplementary data associated with this article can be found, in the online version, at doi:10.1016/j.combustflame.2011.05.007.

References

- [1] H.J. Curran, P. Gaffuri, W.J. Pitz, C.K. Westbrook, Combust. Flame 114 (1998) 149–177.
- [2] C.K. Westbrook, W.J. Pitz, O. Herbinet, H.J. Curran, E.J. Silke, Combust. Flame 156 (2009) 181–199.
- [3] H.J. Curran, P. Gaffuri, W.J. Pitz, C.K. Westbrook, Combust. Flame 129 (2002) 253–280.
- [4] M.A. Oehlschlaeger, J. Steinberg, C.K. Westbrook, W.J. Pitz, Combust. Flame 156 (2009) 2165–2172.
- [5] C.K. Westbrook, W.J. Pitz, J.E. Boercker, H.J. Curran, J.F. Griffiths, C. Mohamed, M. Ribacour, Proc. Combust. Inst. 29 (2002) 1311–1318.
- [6] C.K. Westbrook, W.J. Pitz, H.J. Curran, J. Boercker, E. Kunrath, Int. J. Chem. Kinet. 33 (12) (2001) 868–877.
- [7] M. Mehl, G. Vanhove, W.J. Pitz, E. Ranzi, Combust. Flame 155 (4) (2008) 756–772.
- [8] M. Mehl, W.J. Pitz, C.K. Westbrook, K. Yasunaga, C. Conroy, H.J. Curran, Proc. Combust. Inst. 33 (2011) 201–208.
- [9] M. Mehl, W.J. Pitz, C.K. Westbrook, H.J. Curran, Proc. Combust. Inst. 33 (2011) 193–200.
- [10] E.J. Silke, W.J. Pitz, C.K. Westbrook, J. Phys. Chem. A 111 (2007) 3761–3775.
- [11] W.J. Pitz, C.V. Naik, T.N. Mhaoduin, C.K. Westbrook, H.J. Curran, J.P. Orme, J.M. Simmie, Proc. Combust. Inst. 31 (2007) 267–275.
- [12] M. Mehl, W.J. Pitz, M. Sjöberg, J.E. Dec, SAE 2009 International Powertrains, Fuels and Lubricants Meeting, SAE Paper No. 2009-01-1806, Florence, Italy.
- [13] C.K. Westbrook, W.J. Pitz, M. Mehl, H.J. Curran, Proc. Combust. Inst. 33 (2011) 185–192.
- [14] W.J. Pitz, C.J. Mueller, Prog. Energy Comb. Sci. 37 (2011) 330–350.
- [15] M. Alnajjar, B. Cannella, H. Dettman, C. Fairbridge, J. Franz, T. Gallant, R. Gieleciak, D. Hager, C. Lay, S. Lewis, M. Ratcliff, S. Sluder, J. Storey, H. Yin, B. Zigler, CRC Report No. FACE-1, Coordinating Research Council, Inc., Alpharetta, GA, 2010.
- [16] B.L. Smith, T.J. Bruno, J. Propul. 24 (3) (2008) 619–623.
- [17] B.L. Smith, T.J. Bruno, Ind. Eng. Chem. Res. 46 (1) (2007) 310–320.
- [18] G. Knothe, Prog. Energ. Combust. Sci. 36 (2010) 364–373.
- [19] T.J. Bruno, E. Baibourine, Energy Fuels 25 (4) (2011) 3565–3571.
- [20] R. Wilk, W.J. Pitz, C.K. Westbrook, S. Addagarla, D.L. Miller, N.P. Cernansky, R.M. Green, Proc. Combust. Inst. 23 (1990) 1047–1053.
- [21] T. Ogura, Y. Nagumo, A. Miyoshi, M. Koshi, Energy Fuels 21 (2007) 130–135.
- [22] M.A. Oehlschlaeger, D.F. Davidson, J.T. Herbon, R.K. Hanson, Int. J. Chem. Kinet. 36 (2) (2004) 67–78.
- [23] D. Healy, N.S. Donato, C.J. Aul, E.L. Petersen, C.M. Zinner, G. Bourque, H.J. Curran, Combust. Flame 157 (2010) 1540–1551.
- [24] A. Burcat, E. Olchanski, C. Sokolinski, Combust. Sci. Technol. 147 (1999) 1–37.
- [25] J.F. Griffiths, J.P. MacNamara, C.G.W. Sheppard, D.A. Turton, B.J. Whitaker, Fuel 81 (2002) 2219–2225.
- [26] E.J. Silke, H.J. Curran, J.M. Simmie, Proc. Combust. Inst. 30 (2005) 2639–2647.
- [27] M.S.P. Kahandawala, M.J. DeWitt, E. Corporan, S.S. Sidhu, Energy Fuels 22 (2008) 3673–3679.
- [28] S.M. Sarathy, C. Yeung, C.K. Westbrook, W.J. Pitz, M. Mehl, M.J. Thomson, Combust. Flame 158 (2010) 1277–1287.
- [29] ASTM D 6890, ASTM International, West Conshohocken, PA, 2007.
- [30] L.N. Allard, N.J. Hole, G.D. Webster, T.W.I. Ryan, D. Ott, A. Beregszazy, C.W. Fairbridge, J. Cooley, K. Mitchell, E.K. Richardson, N.G. Elliot, D.J. Rickeard, SAE Tech. Pap. 971636, 1997.
- [31] L.N. Allard, G.D. Webster, T.W.I. Ryan, A. Matheaus, G. Baker, A. Beregszazy, H. Read, K. Mortimer, G.J. Jones, SAE Tech. Pap. 2001013527, 2001.
- [32] M.V. Johnson, S.S. Goldsborough, Z. Serinyel, et al., Energy Fuels 23 (2009) 5886–5898.
- [33] J. Moc, G. Black, J.M. Simmie, H.J. Curran, AIP Conf. Proc. 1148 (2009) 161–164.
- [34] W.S. McGivern, I.A. Awan, W. Tsang, J.A. Manion, J. Phys. Chem. A 112 (2008) 6908–6917.
- [35] W. Tsang, J.A. Walker, J.A. Manion, Proc. Combust. Inst. 32 (2007) 141–148.

- [36] W. Tsang, W.S. McGivern, J.A. Manion, Proc. Combust. Inst. 32 (2009) 131–138.
- [37] I.A. Awan, W.S. McGivern, W. Tsang, J.A. Manion, J. Phys. Chem. A 114 (2010) 7832–7846.
- [38] L. Zhu, J.W. Bozzelli, L.M. Kardos, J. Phys. Chem. A 111 (2007) 6361–6377.
- [39] G.E. Quelch, M.M. Gallo, M.Z. Shen, Y.M. Xie, H.F. Schaefer, D. Moncrieff, J. Am. Chem. Soc. 116 (11) (1994) 4953–4962.
- [40] J.D. Desain, S.J. Klippenstein, J.A. Miller, C.A. Taatjes, J. Phys. Chem. A 107 (22) (2003) 4415–4427.
- [41] C.Y. Sheng, J.W. Bozzelli, A.M. Dean, A.Y. Chang, J. Phys. Chem. A 106 (2002) 7276–7293.
- [42] E.J. Silke, W.J. Pitz, C.K. Westbrook, M. Ribaucour, J. Phys. Chem. A 111 (19) (2007) 3761–3775.
- [43] E.R. Ritter, J.W. Bozzelli, Int. J. Chem. Kinet. 23 (1991) 767–778.
- [44] S.W. Benson, Thermochemical Kinetics, 2nd ed., Wiley, New York, 1976.
- [45] T.H. Lay, J.W. Bozzelli, A.M. Dean, E.R. Ritter, J. Phys. Chem. 99 (1995) 14514–14527.
- [46] J.W. Bozzelli, Personal Communication, New THERM Version, 2003.
- [47] L.S. Tee, S. Gotoh, W.E. Stewart, Ind. Eng. Chem. Fundam. 5 (3) (1966) 356–363.
- [48] H. Wang, M. Frenklach, Combust. Flame 96 (1994) 163–170.
- [49] A.T. Holley, X.Q. You, E. Dames, H. Wang, F.N. Egolfopoulos, Proc. Combust. Inst. 32 (2009) 1157–1163.
- [50] B.I. Lee, M.G. Kesler, AIChE J. 21 (1975) 510–527.
- [51] I. Owczarek, K. Blazej, J. Phys. Chem. Ref. Data 32 (4) (2003) 1411–1427.
- [52] I. Owczarek, K. Blazej, J. Phys. Chem. Ref. Data 35 (4) (2006) 1461–1474.
- [53] S.M. Sarathy, M.J. Thomson, W.J. Pitz, T. Lu, Proc. Combust. Inst. 33 (2011) 399–405.
- [54] R. Bosque, J. Sales, J. Chem. Inf. Comput. Sci. 42 (2002) 1154–1163.
- [55] D.R. Lide (Ed.), CRC Handbook of Chemistry and Physics, 87th ed., Taylor and Francis, Boca Raton, FL, 2007.
- [56] A.L. McClellan, Tables of Experimental Dipole Moments, Freeman, San Francisco, 1963.
- [57] C. Ji, E. Dames, Y.L. Wang, H. Wang, F.N. Egolfopoulos, Combust. Flame 157 (2010) 277–287.
- [58] A. Kelley, W. Liu, Y. Xin, A. Smallbone, C. Law, Proc. Combust. Inst. 33 (2010) 501–508.
- [59] H.-P.S. Shen, M.A. Oehlschlaeger, Combust. Flame 156 (2009) 1053–1062.
- [60] D.R. Haylett, D.F. Davidson, R.K. Hanson, Proc. Combust. Inst. 33 (2011) 167–173.
- [61] E.J. Silke, Ph.D. Thesis, National University of Ireland, Galway, 2005.
- [62] CHEMKIN-PRO Release 15101, Reaction Design, Inc., San Diego, CA, 2010.
- [63] S. Dooley, H.J. Curran, J.M. Simmie, Combust. Flame 153 (2008) 2–32.
- [64] P. Dagaut, M. Cathonnet, J.P. Rouan, R. Foulquier, A. Quilgars, J.C. Boettner, F. Gaillard, H. James, J. Phys. E: Instrum. 19 (1986) 207–209.
- [65] G. Dayma, S.M. Sarathy, C. Togbé, C. Yeung, M. Thomson, P. Dagaut, Proc. Combust. Inst. 33 (1) (2011) 1037–1043.
- [66] P. Dagaut, M. Reuillon, M. Cathonnet, D. Presvots, Chromatographia 40 (1995) 147–154.
- [67] O. Herbinet, S. Bax, P.-A. Glaude, V. Carré, F. Battin-Leclerc, Fuel 90 (2) (2011) 528–535.
- [68] H.B. Palmer, B.E. Knox, ARS J. 31 (1961) 826–828.
- [69] H.K. Ciezki, G. Adomeit, Combust. Flame 93 (1993) 421–433.
- [70] U. Pfahl, K. Fieweger, G. Adomeit, Proc. Combust. Inst. 26 (1996) 781–789.
- [71] M. Chaos, F.L. Dryer, Int. J. Chem. Kinet. 42 (2010) 143–150.
- [72] A.T. Holley, Y. Dong, M.G. Andac, F.N. Egolfopoulos, Combust. Flame 144 (2006) 448–460.
- [73] A.T. Holley, Y. Dong, M.G. Andac, F.N. Egolfopoulos, T. Edwards, Proc. Combust. Inst. 31 (2007) 1205–1213.
- [74] P.S. Veloo, Y.L. Yang, F.N. Egolfopoulos, C.K. Westbrook, Combust. Flame 157 (2010) 1989–2004.
- [75] C.K. Wu, C.K. Law, Proc. Combust. Inst. 20 (1984) 1941–1949.
- [76] Y.L. Wang, A.T. Holley, C. Ji, F.N. Egolfopoulos, T.T. Tsotsis, H.J. Curran, Proc. Combust. Inst. 32 (2009) 1035–1042.
- [77] S.G. Davis, C.K. Law, Combust. Sci. Technol. 140 (1998) 427–449.
- [78] P.S. Veloo, F.N. Egolfopoulos, Combust. Flame 158 (2011) 501–510.
- [79] P.S. Veloo, F.N. Egolfopoulos, Proc. Combust. Inst. 33 (2011) 987–993.
- [80] T.F. Lu, C.K. Law, Proc. Combust. Inst. 30 (2005) 1333–1341.
- [81] Z. Luo, T. Lu, M. Maciaszek, S. Som, D. Longman, Energy Fuels 24 (2010) 6283–6293.
- [82] T.F. Lu, C.K. Law, Combust. Flame 144 (2006) 24–36.
- [83] A.E. Lutz, R.J. Kee, J.A. Miller, Technical Report SAND87-8248, Sandia National Laboratories, 1987.
- [84] P. Glarborg, R. Kee, J. Grcar, J. Miller, SAND86-8209, Sandia National Laboratories, 1986.
- [85] T.F. Lu, C.K. Law, Prog. Energy Combust. Sci. 35 (2009) 192–215.
- [86] K. Seshadri, T.F. Lu, O. Herbinet, S.B. Humer, U. Niemann, W.J. Pitz, R. Seiser, C.K. Law, Proc. Combust. Inst. 32 (2009) 1067–1074.
- [87] X.L. Zheng, T.F. Lu, C.K. Law, Proc. Combust. Inst. 31 (2007) 367–375.
- [88] R. Sankaran, E.R. Hawkes, J.H. Chen, T.F. Lu, C.K. Law, Proc. Combust. Inst. 31 (2007) 1291–1298.
- [89] K. Seshadri, F. Williams, Int. J. Heat Mass Transfer 21 (1978) 251–253.
- [90] V. Giovangigli, M.D. Smooke, Combust. Sci. Technol. 53 (1) (1987) 23–49.
- [91] M. Nishioka, C.K. Law, T. Takeno, Combust. Flame 104 (3) (1996) 328–342.
- [92] A.J. Smallbone, W. Liu, C.K. Law, X.Q. You, H. Wang, Proc. Combust. Inst. 2009) 1245–1252.
- [93] J. Biet, M.H. Hakka, V. Warth, P.-A. Glaude, F. Battin-Leclerc, Energy Fuels 22 (2008) 258–2269.
- [94] J.E. Dec, SAE Paper 970873, 1997, pp. 1–30.
- [95] M.J. Murphy, J.D. Taylor, R.L. McCormick, Compendium of Experimental Cetane Number Data, NREL/SR-540-36805, National Energy Renewable Laboratory, Golden, Colorado, USA, 2004.
- [96] S. Dooley, S.H. Won, M. Chaos, J. Heyne, Y. Ju, F.L. Dryer, K. Kumar, C.-J. Sung, H. Wang, M.A. Oehlschlaeger, R.J. Santoro, T.A. Litzinger, Combust. Flame 157 (2010) 2333–2339.
- [97] C.V. Naik, K.V. Puduppakkam, A. Modak, E. Meeks, Y.L. Wang, Q. Feng, T.T. Tsotsis, Combust. Flame 158 (2011) 434–445.
- [98] P. Gokulakrishnan, M.A. Klassen, R.J. Roby, ASME Turbo Expo #GT2008-51211, Berlin, Germany, 2008.
- [99] Y. Ra, R. Reitz, Combust. Flame 158 (2011) 69–90.
- [100] Y. Ra, R. Reitz, Combust. Flame 155 (2008) 713–738.